Deep–Sea Research I 210 (2024) 104342

Contents lists available at ScienceDirect

Deep-Sea Research Part I

journal homepage: www.elsevier.com/locate/dsri

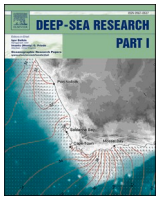

Multidisciplinary characterisation of the biodiversity, geomorphology, oceanography and glacial history of Bowditch Seamount in the Sargasso Sea

Lea-Anne Henry [a,*], Igor Yashayaev [b], Claude Hillaire-Marcel [c], F. Javier Murillo [b], Ellen Kenchington [b], Struan Smith [d], Jenny Maccali [e], Jill Bourque [f], Louis L. Whitcomb [g], J. Murray Roberts [a]

[a] University of Edinburgh, School of GeoSciences, James Hutton Road, Edinburgh, EH9 3FE, United Kingdom
[b] Department of Fisheries and Oceans, Bedford Institute of Oceanography, 1 Challenger Drive, Dartmouth, Nova Scotia, B2Y 4A2, Canada
[c] Geotop Research Center and Département des Sciences de La Terre et de L'atmosphère, Université Du Québec à Montréal, Montréal, Québec, H3C 3P8, Canada
[d] Natural History Museum, Bermuda Aquarium, Museum and Zoo, 40 N Shore Road, Hamilton Hamilton Parish, FL 04, Bermuda
[e] Department of Earth Sciences and Bjerknes Centre for Climate Research, University of Bergen, Bergen, N-5007, Norway
[f] U.S. Geological Survey, Wetland and Aquatic Research Center, 7920 NW 71st Street, Gainesville, FL, 32653, USA
[g] Johns Hopkins University, Department of Mechanical Engineering, 3400 N Charles Street, Baltimore, MD, 21218, USA

ARTICLE INFO

Keywords:
Sargasso sea
Seamounts
Corals
Vulnerable marine ecosystems
Climate change
Labrador sea water

ABSTRACT

The first multidisciplinary characterisation of Bowditch Seamount in the Sargasso Sea was conducted to provide new baseline knowledge of the biodiversity, geomorphology, oceanography and glacial history of this seamount. A dropframe camera transect 1483–1562 m deep on the seamount documented 77 megafaunal taxa including Vulnerable Marine Ecosystem indicator taxa such as sponges, cold-water corals, and stalked crinoids. Seabed terrain analysis of multibeam echosounder data showed species varied significantly along this transect in response to local geomorphological variability (R^2_{adj} = 31%, p < 0.0001), with changes in seafloor relief and substrata driving species composition over the seamount. ^{14}C-calibrated and ^{230}Th-ages of fossil corals (*Desmophyllum dianthus*) collected by Van Veen grabs 1517 m deep showed corals thrived on the seamount ~24 ka BP and ~17 ka BP. Abrupt excursions between higher and lower radiogenic ε_{Nd}-composition values of the skeletons suggested that *D. dianthus* persisted on the seamount over times of southern source water input and detrital sediments from the melting Laurentide Ice Sheet, respectively. In agreement with other studies from the western North Atlantic, living *D. dianthus* were absent in the contemporary setting at these depths, and suggest a significant re-organisation of the seamount community since the deglacial when ice-rafted debris of carbonates likely resulted in a lower aragonite compensation depth allowing *D. dianthus* to proliferate at deeper depths. New conductivity-depth-temperature profiling revealed the seamount at these depths is now bathed by highly oxygenated Labrador Sea Water (LSW) formed at high latitudes. Co-analysis of a newly constructed 70-year long time series of temperature and salinity for the Labrador Sea and Bermuda regions revealed a 10-year transit time from high latitudes to Bowditch Seamount. This multidisciplinary approach shows how geomorphology drives local biodiversity patterns, but also how upstream climatic forcing in subpolar regions may influence Bermuda's subtropical seamount ecosystem.

1. Introduction

Seamount ecosystems comprise topographically elevated areas, which rise more than 1 km above the seafloor and that were once geologically active. These geomorphological features interact with prevailing ocean currents in different ways, such that many seamounts support diverse and highly productive ecosystems (Clark et al., 2012, 2021). Seamounts also support human livelihoods and food security, particularly through commercial and small-scale fisheries (Pitcher et al., 2010; Ressurreição and Giacomello, 2013).

* Corresponding author.
E-mail address: l.henry@ed.ac.uk (L.-A. Henry).

https://doi.org/10.1016/j.dsr.2024.104342
Received 8 June 2023; Received in revised form 10 June 2024; Accepted 10 June 2024
Available online 12 June 2024

Patterns of biological diversity on an individual seamount are a product of its geological history, environmental setting, biological (species) interactions and larval dispersal, and human activities, all of which are scale-dependent over space and time. Rarely though are these drivers examined simultaneously to explain contemporary patterns. Focussing on just the environmental setting, the sheer physicality of a seamount rising more than 1 km from the seafloor means that benthic ecosystems may transition through several water masses. Each water mass has its own physicochemical signature in, e.g., water temperature, salinity, oxygen and nutrient concentrations, calcium carbonate saturation levels, and food supply. Notably, many of these parameters are also likely to be significantly altered by climate change by the end of this century in many regions (Sweetman et al., 2017; Puerta et al., 2020), which will have implications for seamount biodiversity.

Besides water mass properties, we know that sediment type and geomorphology also exert strong control on seamount species richness, biomass, density, and community composition. Together, these environmental gradients occurring over a single seamount significantly affect biodiversity over scales from centimetres to kilometres (Henry et al., 2014; Boschen et al., 2015; Victorero et al., 2018; Morgan et al., 2019; Auscavitch et al., 2020). For example, the density of larger sessile megabenthos often peaks in areas of exposed bedrock or other outcrops (Grigg, 1997; Ramiro Sánchez et al., 2019), whereas more unconsolidated sediments (scree) typically host assemblages characterised by smaller more mobile megabenthic species (Clark and Bowden, 2015). Sometimes, these changes in sediment type also correlate with topographic changes, e.g., in slope, rugosity, and curvature, which together influence diversity patterns (Du Preez et al., 2016; De la Torriente et al., 2018).

Understanding the past, present, and future state of seamounts requires multidisciplinary and multiscale approaches to improve how we then manage and conserve seamount resources. Many international agreements and institutions now recognise the importance of conservation and sustainable use of seamounts, and this makes it incumbent for scientists and authorities to take stock of and report on seamount communities, biological resources and any vulnerabilities to anthropogenic activities and climate change. Management guidance and technical criteria have been developed to assist States and Regional Fisheries Management Organisations (RFMOs) in implementing United Nations General Assembly (UNGA) resolution 61/105, which called for measures to identify and protect vulnerable marine ecosystems (VMEs; FAO, 2009) such as deep-sea sponge grounds, cold-water coral reefs, and coral gardens. Besides numerous accounts of VMEs and VME indicator taxa on seamounts worldwide, an entire seamount may in its own right, constitute a VME (FAO, 2009; Watling and Auster, 2017). With little capacity for recovery from significant adverse impacts caused by bottom trawling (Clark et al., 2019) and knowing that even lost fishing gear poses threats (Du Preez et al., 2020) all along a backdrop of rapid climate change, it is vital we take every opportunity to improve our understanding of seamounts.

1.1. Bermuda's seamounts

Unlike many seamounts that have been affected by human activities, Bermuda's chain of seamounts in the western North Atlantic remains relatively unimpacted and there is evidence for the occurrence of VMEs. Bermuda's exclusive economic zone (EEZ) extends over the Bermuda Rise and includes three seamounts: Challenger Bank, Plantagenet (or Argus) Bank, and Bowditch Seamount (Coates et al., 2013). Crescent Seamount is located further to the north and west, while the Muir Seamount chain, Siboney and George Seamounts are located to the northeast.

In 1873, HMS *Challenger* conducted depth soundings and dredging around Challenger and Plantagenet (Argus) Banks. Later, Fricke and Meischner (1985) conducted submersible surveys on the Bermuda pedestal and Challenger and Plantagenet (Argus) Banks and reported ahermatypic coral communities at 200 m water depth. Crewed submersible missions in 1993 and 1997 used the Deep Submergence Vehicle DSV *Alvin* (Woods Hole Oceanographic Institute) and the Canadian Navy's Submersible Diver Lockout vehicle *SDL-1* to collect seamount fauna, sampling hydroids down to depths of 3550 and 376 m, respectively (Calder, 1998). Iliffe (2012) conducted dive surveys around Bermuda and on Challenger Bank to 136 m with extensive photo-documentation and collection of corals and sponges. Intensive studies were performed on Bermuda and Plantagenet Bank in 2016 as part of the NEKTON Project using submersibles and dive surveys that described rich benthic and fish communities down to 300 m (Stefanoudis et al., 2019a, 2019b). Limited coral collections have been done at deeper depths, however Adkins et al. (2004) reported on the growth rate of the scleractinian *Enallopsammia rostrata* collected by DSV *Alvin* on the north slope of Bermuda at 1410 m in 2001. Adkins (2003) also conducted intensive mapping and sample collection on the Muir seamounts, documenting extensive coral and associated faunal communities (Canache, 2007; Robinson et al., 2007; Cho, 2008; Thoma et al., 2009; Cho and Shank, 2010). Notably, the only account of biodiversity on Bowditch Seamount concerns the Hydrozoa collected by dredge and Van Veen grabs during the R/V *Meteor* 35/2 mission in May 1996 (Hemleben et al., 1998), in which four species were recorded (Calder, 1998, 2000).

Bermuda's EEZ and the Sargasso Sea more generally are increasingly at risk from illegal fishing, mining and dumping, but local authorities have limited enforcement capacity (Government of Bermuda, 2022). In the future, commercial deep seabed mining for non-living seafloor resources in the region such as polymetallic sulphides, nodules, gas hydrates, and cobalt-rich manganese crust (Pratt, 1962; Addy, 1979; Adkins, 2003) could occur in large quantities (Parson and Edwards, 2011). Unsustainable exploitation would compromise ecosystem services that Bermudians gain from these seamounts (Hallett, 2011). Taxa that indicate the occurrence of VMEs on the Muir seamounts include antipatharians, chrysogorgiids, bamboo corals, and the colonial reef-building scleractinian *Enallopsammia rostrata* as well as a number of sponge, bryozoan, and crinoid taxa (Adkins, 2003) including a species new to science, the carnivorous cladorhizid sponge *Abyssocladia polycephalus* (Hestetun et al., 2016). However, it is critical to survey and identify VMEs across more of Bermuda's seamounts and to understand what controls seamount biodiversity to ensure that future human activities do not degrade the very features that support VMEs.

1.2. Climate change and oceanographic observations around Bermuda

In the coming decades, cumulative impacts of climate change will also likely alter the distribution and diversity of VME indicator taxa on Bermuda's seamounts, with worst-case emission scenarios potentially having devastating consequences for many deep-sea fish and cold-water corals in the North Atlantic (Morato et al., 2020). The contemporary physicochemical and biological setting of the Sargasso Sea region has been well characterised and is monitored by the long-running Bermuda Atlantic Time-series Study (BATS) and the Hydrostation S time series, and the profiling Argo floats including Deep Argo. These international efforts have provided scientists with sustained *in situ* monthly observations since 1988, biweekly observations since the 1950s (Phillips and Joyce, 2007), and continuously transmitted Argo profiles since 2002 (Wong et al., 2020), respectively. These time series have helped to reveal how atmospheric oscillations in the open North Atlantic have re-shaped Bermuda's ecosystems over many decades (Bates et al., 2012; Lomas et al., 2013), with today's conditions being closely coupled to large-scale atmospheric processes, e.g., the North Atlantic Oscillation (NAO) and the El Niño Southern Oscillation (ENSO). Evidence for upper-ocean deoxygenation, decreasing pH and warming water temperatures is emerging, and these have likely impacted biological phenomena such as coral calcification, at least in Bermuda's shallower waters (Bates, 2017).

Impacts of oceanographic shifts occurring in distant geographical regions on Bermuda's deep-sea ecosystems are considered less often. For

Bermuda's seamounts, an important active teleconnection to the subpolar North Atlantic is provided by the circulation of Labrador Sea Water (LSW), an intermediate-depth water mass formed in response to high winter surface heat losses in the Labrador Sea (Yashayaev et al., 2007). The cooling and mixing of the upper layer waters leads to formation of cold, fresh, dense and oxygen-rich LSW and forms multiyear LSW classes that progressively increase in depth, density, thickness and volume year by year (Yashayaev and Loder, 2016, 2017). LSW is transported by different segments of the deep-ocean circulation to the eastern North Atlantic (Yashayaev et al., 2007; Gonçalves Neto et al., 2020) and to the Sargasso Sea (Curry et al., 1998; Chomiak et al., 2022). The equatorward transport of this water mass is performed through its entrainment in the southward-flowing Deep Western Boundary Current (DWBC: Le Bras et al., 2017; Feucher et al., 2019) and by joining and following the internal ocean circulation pathways, resulting in LSW entering and spreading across the North Atlantic Subtropical Gyre (Chomiak et al., 2022).

With respect to climate change, LSW transport is also responsible for the storage and utilisation of anthropogenic CO_2 in deep layers (Rhein et al., 2017). Deeper in the water column, some anthropogenic tracer-based linkages have also been made with Denmark Strait Overflow Water (DSOW), an abyssal water mass, originating from the polar overflow entering the subpolar North Atlantic through the deep trenches in the Denmark Strait (Yashayaev and Dickson, 2008; Smith et al., 2016). Thus, upstream changes in high latitude convection processes and atmospheric dynamics driving LSW properties could modulate temporal variability in the water masses bathing Bermuda's deep-sea ecosystems including seamount communities.

1.3. Palaeoceanographic reconstructions

The influence of atmospheric and oceanic teleconnections on the contemporary seamount ecosystems of Bermuda have not been studied. However, palaeoceanographic reconstructions from solitary deep-sea scleractinian corals on the Muir seamount range, New England and Corner Rise seamount chains reveal a turbulent geological history, with drastic re-organisations in water mass properties and circulation features since the last glacial maximum (LGM) ~21 kya. Geochemical analysis of the aragonitic calcium carbonate skeleton of *Desmophyllum dianthus* documented a "boom and bust" phenomenon: solitary corals proliferated over a wide depth range (1100–2600 m) during the deglacial, whereas today the species is more narrowly restricted (around 1100 m) at these latitudes (Robinson et al., 2007; Thiagarajan et al., 2013). Contemporary evidence for this ancient waxing and waning takes the form of vast coral graveyards, or "death assemblages", of fossilised *D. dianthus* in the region (Lapointe et al., 2020), first documented by Pratt (1962, 1967) on the Muir seamounts. The turbulent geological past recorded by fossil corals on the Muir range (Adkins, 2003; Eltgroth et al., 2006; Thiagarajan et al., 2013) was possibly driven by abrupt glacial-deglacial shifts in food supply and productivity, oxygen concentrations and aragonite saturation (Thiagarajan et al., 2013). If corals from more of Bermuda's seamounts can be analysed, then convergence on a general paradigm to explain the boom and bust might result, along with a better understanding of teleconnections from subpolar regions.

1.4. A multidisciplinary scientific approach to aid planning and policy implementation

Bermuda recently launched its national marine spatial planning (MSP) process, the "Blue Ocean Prosperity Programme" (Government of Bermuda, 2022). Information from Adkins (2003) and predictive species distribution models (Tittensor et al., 2009; Yesson et al., 2012) were used to justify the proposed protection of the entire Muir Seamount range as a fully protected marine protected area (MPA) and partial protection for the Crescent Seamount. However, with the limited understanding of how seamount biodiversity is coupled to environmental variables, it is unclear what impacts climate change and oceanographic variability will bring to these seamounts. Thus, new multidisciplinary missions to Bermuda's seamounts have a timely opportunity to contribute information to support the implementation of international and national obligations such as those to identify VMEs, and to support Bermuda's MSP process.

The present study aimed to provide the first multidisciplinary characterisation of the biodiversity, geomorphology, oceanography and glacial history of Bowditch Seamount to assist Bermuda's maritime spatial planning and related management processes. To do so, our multidisciplinary approach integrated several sea-going research expeditions to map the seafloor, characterise seamount biodiversity, reconstruct its glacial-deglacial history, and complete full oceanographic sections between Bermuda and Atlantic Canada to understand local and large-scale connectivity between the export of LSW and Bermuda's seamounts.

2. Materials and methods

2.1. Study location and oceanographic setting

Bowditch Seamount is a submerged volcanic cone approximately 12 km in diameter, located approximately 39 km NNE of the Bermuda Platform (Fig. 1; top panel).

The cone formed 33–34 mya (Vogt and Jung, 2007) but became volcanically extinct by the Oligocene. Today, the shallowest of the summits on Bowditch reaches 1242 m below the sea surface (GEBCO, 2023), with its flanks extending into waters nearly 4000 m deep. The bathyal seamount fauna are therefore likely to be strongly affected by physiochemical processes in remote water mass sources such as LSW due to its deep water circulation.

Bowditch is located in the western Tropical North Atlantic biogeographic province (Spalding et al., 2007) in the highly oligotrophic setting of the Sargasso Sea. The winter mixed layer of the Sargasso Sea is usually as deep as 700–1000 m. Underlain by the main thermocline, this upper layer is mainly occupied by North Atlantic Subtropical Mode Water (STMW), also known as Eighteen Degree Water (EDW) or Sargasso Sea Water. A secondary thermocline develops in summer under a much shallower mixed layer typically less than 20 m (Steinburg et al., 2001; Fawcett et al., 2014).

Large-scale circulation patterns at 1000 m (Fig. 2) are important to our understanding of the intermediate-depth circulation in the North Atlantic and at Bowditch, even though LSW is mainly found deeper than 1000 m on the seamount. There are two reasons for this. First, the only massive dataset of direct flow measurements is based on Argo float displacements at their parking depth is predominantly at 1000 m, and second, currents at this depth are highly correlated with those as deep as 2000 m (Chomiak et al., 2022).

Bordering the Sargasso Sea along its northern boundary edge is the Gulf Stream (GS). Approximately at the latitude of Cape Hatteras, the GS changes its prevailing direction, heading eastwardly towards the Newfoundland Basin. At the GS branching point in the Newfoundland Basin, a part of this current becomes the North Atlantic Current (NAC). An important feature of the ocean circulation south of Nova Scotia is the Slope Water Gyre. It is bounded by the Slope Current on its inshore northern flank, and by GS on the offshore southern one. The Slope Water Gyre mixes and recirculates the GS and slope waters. The GS and NAC, collectively constitute the upper limb of the Atlantic Meridional Overturning Circulation (AMOC). However, only the NAC part of the GS follows this limb toward Europe, while the other branches retain GS water at mid- and lower latitudes (Chomiak et al., 2022). The first branch to separate from the main GS flow forms the GS recirculation gyre. Once departed from the GS, this flow turns south off the Grand Banks, completes its clockwise turn, and heads towards Bermuda where the GS recirculation flow eventually mixes with Sargasso Sea Water, becoming nearly indistinguishable from the latter.

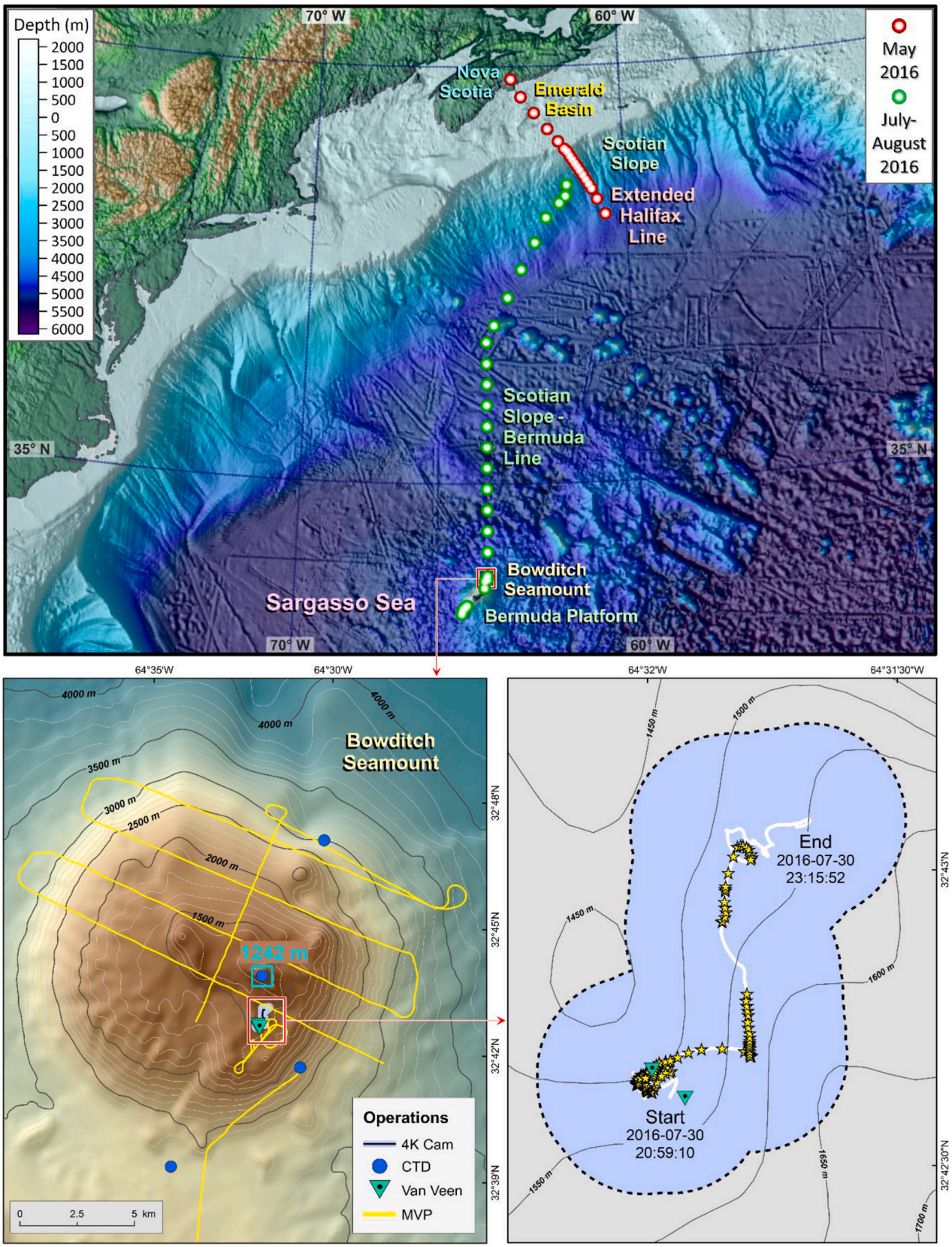

Fig. 1. Geographical setting and sampling locations of Bowditch Seamount. Locations of oceanographic profiles on the Extended Halifax Line and Scotian Slope - Bermuda Line in May 2016 and July–August 2016 (top panel, red and green circles, respectively); locations of the 4K camera transect CON173, Van Veen benthic sampling, CTD and MVP profiles in relation to Bowditch Seamount with the summit indicated by a red box (bottom left panel); zoomed in 4K camera transect CON173 with a 300 m buffer (light blue) centered on the transect line (white) with camera stations (yellow stars) and the 2 Van Veen stations (bottom right panel). Depth contours are indicated.

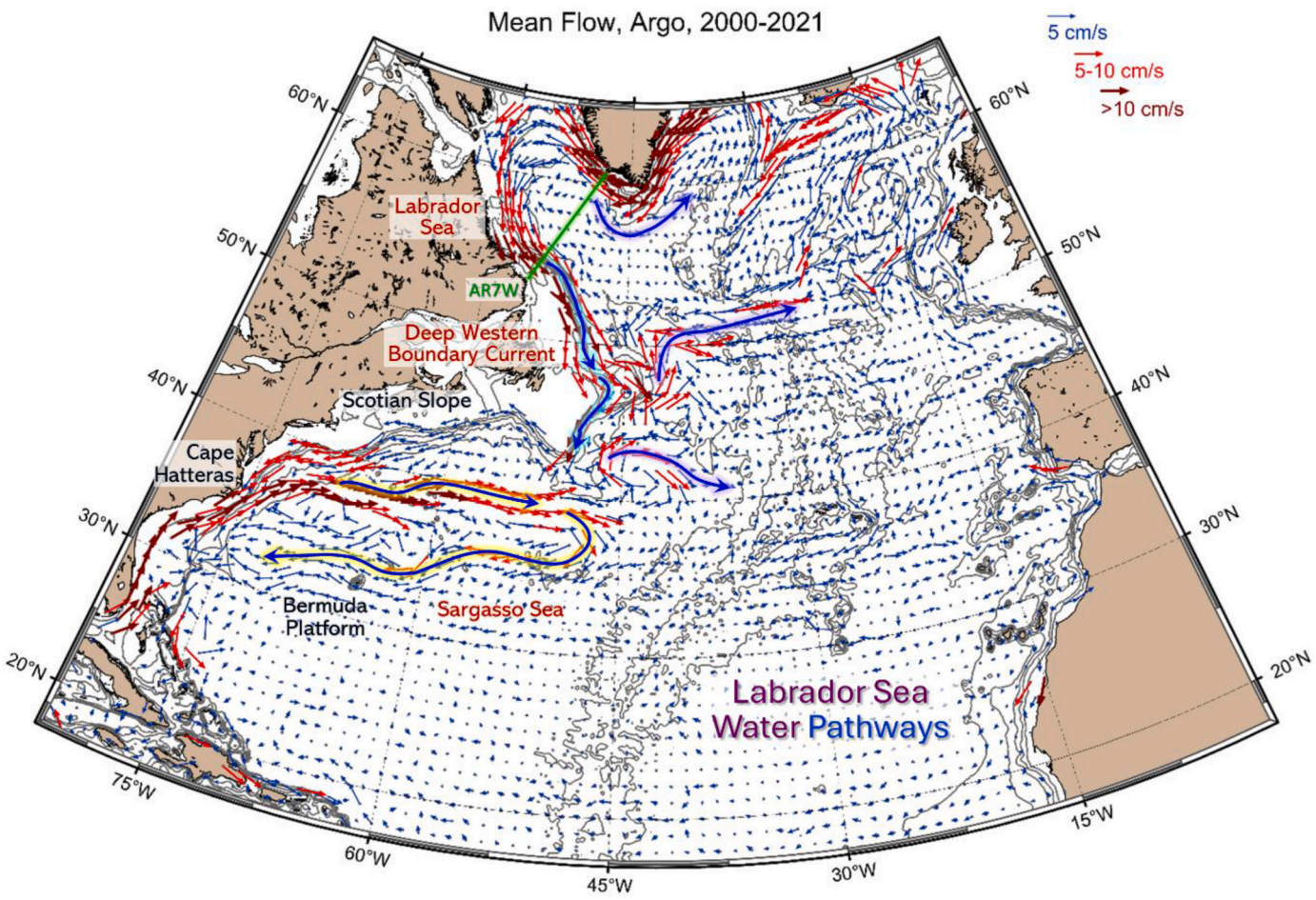

Fig. 2. Mean current flow and speeds at 1,000m water depth (shallow limit of Labrador Sea Water, LSW) estimated along 1° grids from Argo floats (2000–2021). Also shown is the Atlantic Repeat 7 West (AR7W) line analysed later in the present study to fully reconstruct LSW spreading times.

As noted earlier, the circulation pathways of the intermediate and even deeper waters generally resemble those of the upper currents. A large part of the DWBC (Fig. 2), carrying both LSW and DSOW along the continental slope and rise of North America, departs from the continental slope near Cape Hatteras, ultimately reversing its direction. The flow here turns counter-clockwise to flow back eastwards and form a deep recirculation gyre with the DWBC. The DWBC recirculation gyre is aligned in position with the Slope Water Gyre dominating the upper part of the water column between the Slope Current located over the continental slope and GS. On reaching the tail of the Grand Banks, the eastward deep flow changes its direction again following the GS recirculation at a greater depth, i.e., making a clockwise turn to start heading to Bermuda, and then further west to Abaco (Fig. 2, also Chomiak et al., 2022). Chomiak et al. (2022) revealed the tight connectivity between the LSW transport through DWBC and its recirculation, and upper layer circulation, comprising (the Slope Current, Slope Water Gyre, GS, and GS recirculation. This adds an important link to our supposition that the benthic habitat on Bowditch is sensitive to, and can be strongly affected by changes in the supply of LSW and DSOW to Bermuda's seamounts caused by large-scale shifts in forcing factors and Atlantic Ocean circulation itself. Chomiak et al. (2022) also showed that the path delivering LSW to Bermuda has distinct oceanographic signatures, including flow direction and speed, and signal spreading. Therefore, here we conclude that the water mass formed by deep convection in the Labrador Sea spreads as a whole, retaining its physicochemical signature.

2.2. Reconstruction of water masses at Bowditch Seamount

By combining observations from two back-to-back research missions, we constructed the first ever coast-to-coast section from Atlantic Canada to Bermuda with continuously high spatial resolution, because most seawater property profiles are located within 65 km distance range of their closest neighbours. This section therefore allows us to fully depict all water masses relevant to Bowditch Seamount. This composite transect included two full ocean-depth sections occupied during cruise HUD2016006 (30 April–24 May 2016, Chief Scientist Igor Yashayaev) and cruise HUD2016019 (14 July–16 August 2016, Chief Scientist Ellen Kenchington) on board the CCGS *Hudson*.

The Extended Halifax Line (XHL, along-line distance range 0–450 km, Fig. 1) and the Atlantic Repeat 7 West (AR7W, seen in Fig. 2) line crossing the Labrador Sea from Canada to Greenland were occupied as part of a follow-up to the World Ocean Circulation Experiment (WOCE). Together, these were previously analysed as part of the Deep-Ocean Observation and Research Synthesis (DOORS; Yashayaev et al., 2022; Yashayaev, 2024). The one-time section occupied from the Scotian Slope to Bermuda (distance range 450–1700 km, Fig. 1) can be regarded as an extension of the XHL. A synthesis of fully quality-controlled calibrated conductivity-temperature-depth (CTD) measurements from both lines allowed us to construct the first ever full ocean-depth section connecting Halifax and Bermuda, including Bowditch Seamount.

The segment covering Bowditch Seamount also included data from five CTD casts and three moving vessel profile (MVP) deployments (Fig. 1), which provided measurements of temperature, salinity, density, dissolved oxygen, fluorescence, and chlorophyll *a*. These deployments

were conducted from 29 to 31 July 2016 alongside biological sampling with two Van Veen grabs at 1517 m water depth and a 4K underwater still image camera survey (Kenchington et al., 2017, Fig. 1).

2.3. Labrador Sea Water spreading time to Bermuda

The new composite section was used to place the advective-diffusive processes and variability in the intermediate and deeper waters off Bermuda in the context of the large-scale water mass circulation, interactions and mixing. Such a panoramic view of water mass uniformity and gradient zones allowed us to better define the relevant oceanographic zones under varying influences of the Labrador Sea, Slope Water Gyre, GS and Sargasso Sea. The extended coast-to-coast perspective of seawater characteristics also helps to establish connections between the waters ventilated by winter convection in the Labrador Sea to the waters surrounding Bermuda. These connections were further investigated by co-analysing vertical annual profiles of seawater temperature, salinity and density at two locations – the LSW source, i.e., the central Labrador Sea, and Bermuda, thereby establishing the transit time required for LSW to reach Bermuda's seamounts. The annual profiles were constructed for the two locations based on multiple historical, opportunistic, and sustained datasets as outlined next.

The Labrador Sea datasets analysed in the present study are a collection of historical data, sustained hydrographic occupations of the trans-basin WOCE AR7W line, and Argo profiling floats (Yashayaev and Loder, 2016, 2017; Yashayaev et al., 2022; Yashayaev, 2024). These were supplemented with datasets from the US Coast Guard's Ocean Weather Station Bravo time series (1964–1974), the Bedford Institute of Oceanography (Dartmouth, Canada) surveys (1977–1988), and from international surveying partnerships and data centers (see details in Lazier, 1980; Yashayaev et al., 2007; Kieke and Yashayaev, 2015). Annually-averaged vertical profiles of temperature, salinity and density were constructed for the central Labrador Sea using methods described in Yashayaev et al. (2007) and Yashayaev and Loder (2016) for data spanning the years 1948–2016. All procedures to compile, clean, validate, vertically interpolate, and average the recent and historical hydrographic profiles are outlined by Yashayaev et al. (2022).

For the segments around Bermuda, hydrographic data from Hydrostation S and Bermuda Atlantic Time Series (BATS) programs, nearby oceanographic station data from other sections and programs, CTD and expendable bathythermic (XBT) data collected during the HUD2016019 mission, and Argo float profiles were used to construct the time series of annually-averaged vertical profiles similarly to those constructed for the central Labrador Sea and for the period of 1948–2016 to match the Labrador Sea series.

Using an iterative approach to evaluate and remove the seasonal cycle from irregular observations (Yashayaev and Zveryaev, 2001), we estimated and removed the seasonal cycle where its contribution to the total variance exceeded 10%. As a further step, we computed robust record means and subtracted these from the annual values for each depth level. To compare signals, we then normalized the anomalies, dividing those by the respective trimmed standard deviation computed individually for each depth.

2.4. Biological sampling on Bowditch Seamount

A 4K dropframe camera system (Natural Resources Canada) was deployed on Bowditch (cruise event log number CON173) on July 30, 2016 to collect still images of seamount megabenthos across different terrain and habitat types. The 4K system is lowered approximately 1.8 m above the seafloor using a metal shackle for a drop-weight trigger, which raises and lowers (and triggers the digital stills camera operation) as the ship drifted. Camera operation was monitored using a 12 kHz Knudsen sounder in pinger mode, mounted on the sled for bottom trigger closure. This system used a Canon Rebel Eos Ti 12 megapixel camera with two Canon flashes all enclosed inside an aluminium roll cage. The field of view for each image triggered at the seafloor is roughly 0.47 ± 0.05 m^2 (Beazley et al., 2013). The 4K camera survey was conducted over the southeastern flank of Bowditch along a narrow depth contour in waters 1482–1562 m deep for ~225 min. Assuming a conservatively large 300 m buffer between the ship's position and where the camera was located on the seafloor (Fig. 1), this camera transect covered an area of approximately 1.1 km^2.

Two Van Veen grab samples from 1517 m water depth were also obtained at 32.710585 N 64.533127 W, and 32.70997 N 64.532312 W, respectively. Contents were sorted at sea, with solitary corals being stored at −20 °C for post-cruise onshore faunal identification. These two opportunistic samples permitted at least some limited ground-truthing of the taxonomic identities of some of the smaller fauna that were visible in the 4K images.

2.5. Multibeam SONAR seafloor surveys

The present study also included a second survey to map the geomorphology of a small section of Bowditch Seamount using an autonomous underwater vehicle (AUV). These data were used to quantify seamount topographic variables that could drive variation in the megabenthic communities. The *Sentry* AUV (Woods Hole Oceanographic Institution, Woods Hole, MA, USA; Kaiser et al., 2016) was used to conduct seven high-resolution near-seabed multibeam surveys during the R/V *Atlantic Explorer* (Bermuda Institute of Ocean Sciences, St. George's, Bermuda) cruise AE1823 (Berkowitz et al., 2018) from 22–31 August 2018. Of interest herein were the multibeam data from dives 492, 493, 494, 497, and 498, covering 54.2 km of vehicle survey track length shown in Fig. 3.

Sentry utilized an onboard 400 kHz Teledyne Reson SeaBat 7125 multibeam sonar (Teledyne RESON, Slangerup, Denmark). *Sentry*'s navigation system uses a 300 kHz RDI Doppler velocity log (Teledyne RDInstruments, San Diego, CA, USA) and IXBLUE Phins inertial navigation system (Ixblue SAS, Saint-Germain-en-Lye, France) assisted with a Sonardyne AvTrak2 ultra-short baseline (USBL) acoustic system (Sonardyne International Ltd, Yateley, Hampshire, United Kingdom). During multibeam surveys on Bowditch, *Sentry* adopted an advance velocity 0.65 m s^{-1} and flew survey missions mostly at an altitude of 60–70 m above the seafloor.

2.6. Seafloor terrain analysis

A suite of geomorphological variables was created through seafloor terrain analysis of *Sentry*'s multibeam data of elevation data on a 1m by 1m grid. These geomorphological data were combined with Universal Transverse Mercator (UTM) northing and easting co-ordinates to help quantify spatial variation in geomorphology as well as any unmeasured environmental variables. The full suite of variables was used to quantify how much variability in spatial patterns of seamount species composition measured from the 4K camera can be explained by these variables. ArcGIS 3D Analyst and Spatial Analyst Tools were used in their default modes to calculate slope, aspect (direction of maximum slope, from which we derived easting and northing calculated using sine and cosine transformed aspect, respectively), plan curvature, and profile curvature.

While plan curvature is perpendicular to the direction of the maximum slope, profile curvature is in the direction along the maximum slope, and both influence flow dynamics. Plan curvature relates to areas where currents may converge (curvature is negative) or diverge around the surface (curvature is positive). Profile curvature relates to areas where currents may accelerate (curvature is negative) or decelerate (curvature is positive). Therefore, both plan and profile curvature estimate how current flows in an area, which is relevant to particle transport and deposition including food and larval supply.

The Benthic Terrain Modeler toolbox in ArcMap 10.5 was used to extract additional variables including rugosity (terrain ruggedness), fine-scale bathymetric profile index (BPI) defined by a 5 m radius to

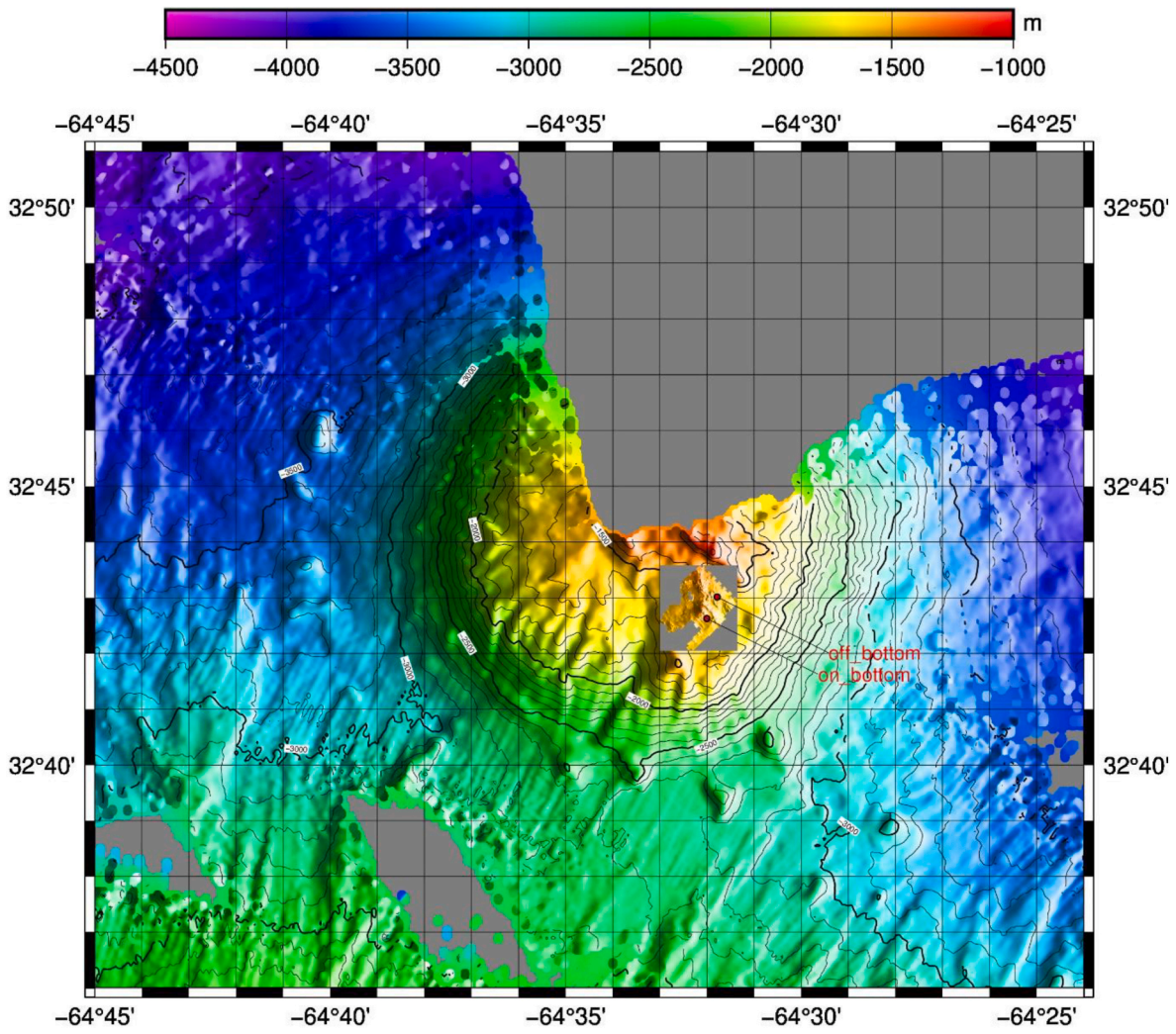

Fig. 3. Near-bottom multibeam survey of *Sentry* dives conducted during cruise AE1823, overlaid on top of historical ship-based multibeam bathymetry of Bowditch Seamount obtained from the National Centers for Environmental Information (NCEI), U.S. National Oceanic and Atmospheric Administration. The higher resolution multibeam from the AE1823 cruise can be seen here bounded by a grey box, inside which the 4K camera stations (indicated by on bottom, and off bottom) are also shown as red circles.

identify smaller raised or depressed features of the seamount's benthic landscape, and a broad-scale BPI defined by a radius 15 m to identify larger raised or depressed features in that landscape.

2.7. Image analysis of seamount megabenthos

The 4K camera deployment (CON173) returned 124 stills images from the northeastern flank of Bowditch, of which 92 images were suitable for analyses. Images were viewed in Picasa viewer v.3.9 post-cruise to classify the predominant substrata and record the presence and absence of morphologically distinct megabenthos in each image. For the present study, megabenthos were living organisms >1 cm in body length, or which could be seen from visual inspection in an image (*sensu* Grassle et al., 1975; Haedrich et al., 1975; Smith and Hamilton, 1983).

Predominant substrata were classified semi-quantitatively using a modified Wentworth scale (Wentworth, 1922) into categories of percent covered by sandy gravel, exposed volcanic basalt rock, and what turned out to be dead (fossil) solitary coral beds. The occurrence of each substratum class was enumerated into increments of five percent up to full coverage of 100% of the seafloor.

Taxonomic identification of megabenthos was conducted independently by two taxonomists, and a consensus on identifications was reached that included reference to Van Veen grab sampling stations that were used to ground-truth some fauna. Pteropods were collected but are pelagic gastropods and likely deposited by currents flowing through the area, thus these were excluded for this benthic analysis.

An environmental-species matrix was created by merging the megabenthos presence/absence data with data on substratum classes and topographic seafloor variables derived from the multibeam surveys and seafloor terrain analyses described earlier.

2.8. Environmental driver analysis

The relationship between environmental variables and community composition of seamount megabenthos was analysed using redundancy analysis (RDA) in XLSTAT v10.1. The method allows the rapid visualisation of important environmental gradients that might be controlling species assembly patterns on Bowditch. RDA also permits the quantification of how much variability in species composition can be explained by these variables, versus other (unmeasured, unknown) factors.

To prepare the environmental-species matrix for RDA analysis, a Hellinger-distance transformation was applied to the species data, which ensured that rarer megabenthos were given lower weights than more common taxa, but which also preserves linear relationships between taxa and any environmental gradients (Legendre and Gallagher, 2001). This final species-environmental matrix contained different

categories of environmental and spatial variables: purely spatial variables (UTM northing and easting of each station), and spatially structured variables (proportions of substrata, slope, rugosity, fine and broad-scale bathymetric position index, aspect, plan, and profile curvature).

2.9. Mineralogy and geochemical analysis

Much of the substrate seen in the 4K camera images was encrusted by black ferromanganese (Fe–Mn) coatings, which faunal identification in the laboratory later revealed was due to presence of mixed solitary scleractinian and colonial octocorals, as noted when Bowditch was dredged in 1996 during the R/V *Meteor* 35 cruise (Hemleben et al., 1998). Once coral live tissues have decomposed, Fe–Mn oxides will form on the surface and coat the carbonate remains of the fossilised coral specimens, giving this dark colour.

Nine solitary corals were collected by the Van Veen grab at sea and radiocarbon analyses were performed. Six of these specimens were analysed for their mineralogy and geochemistry.

2.9.1. Sample cleaning

All mineralogical and isotopic analyses were performed on a well-mixed aliquot from each ground sample, and these corals were later to be identified as the scleractinian *D. dianthus*. Coral samples were preliminary mechanically-cleaned using diamond-coated discs and tips mounted on Dremel™ and Proxxon™ devices. As some coral specimens were fragile and small, the coral septa and theca were both used to obtain enough material. Samples were further cleaned using the chemical cleaning protocol from van de Flierdt et al. (2010) to further remove oxide crust. Samples were then dried, crushed to powder in an agate mortar and stored for subsequent analyses.

2.9.2. X-ray diffraction (XRD) of aragonite and calcite

The present study used XRD to distinguish the two types of calcium carbonate from the six fossil corals. Aragonite peaks at 111 with several lesser peaks, while calcite peaks at 104 with fewer smaller other peaks, thus aragonite content can be expressed in percent of total carbonate from the [111/(111 + 104)] ratios. A first powdered sample aliquot was used for semi-quantitative determinations of these ratios using XRD (Davies and Hooper, 1963) on a Siemens D 5000™ instrument (Co-Kα radiation). Replicate measurements of the laboratory standard mixtures indicated a relative reproducibility better than ±1 % (±1σ).

2.9.3. Stable isotope measurements

Stable carbon isotope ($\delta^{13}C$) composition was measured to help reconstruct the palaeoceanographic setting, for example, depleted $\delta^{13}C$ in deep-sea coral skeletons with respect to equilibrium with ambient seawater can indicate significant uptake of respired CO_2 (Marali et al., 2013). Measurements were made on 100 μg powdered sample aliquots and expressed in δ-units ‰ vs VPDB (Vienne Pee Dee *Belmnitella* reference material; see Hillaire-Marcel et al., 2021) following routine protocols (Hélie and Hillaire-Marcel, 2013). Raw data were corrected using a calibration curve based on two internal reference materials calibrated against NBS 19-LSVEC (see Coplen, 1996; Coplen et al., 2006), with a relative ±1σ uncertainty better than ±0.02‰. Uncertainty of $\delta^{13}C$ values vs VPDB (±1σ) was better than 0.05‰, with all errors propagated for $\delta^{13}C$ values based on replicates of reference carbonate materials analysed simultaneously.

2.9.4. Radiocarbon dating

Reconstructing coral growth history was performed using radiocarbon dating. Aliquots for ^{14}C analyses were prepared and graphitised as described in Crann et al. (2017). Measurements were performed at the A.E. Lalonde AMS Laboratory of Ottawa (Canada) on a 3 MV tandem accelerator mass spectrometer built by High Voltage Engineering. The $^{12,13,14}C^{+3}$ ions were measured at 2.5 MV terminal voltage with Ar-stripping. The fraction vs modern carbon, $F^{14}C$, was calculated according to Reimer et al. (2013) as the ratio of the sample $^{14}C/^{12}C$ ratio to the OXII standard $^{14}C/^{12}C$ ratios (e.g., Wacker et al., 2010) measured in the same data block. Both $^{14}C/^{12}C$ ratios were background-corrected, and the result was corrected for spectrometer and preparation fractionation using the AMS-measured $^{13}C/^{12}C$ ratio normalized to $\delta^{13}C = -25‰$ (VPDB). Conventional radiocarbon ages (i.e., in "Libby's years") were calculated as $-8033\ln(F^{14}C)$ and reported in ^{14}C yr BP (BP = 1950 CE; *sensu* Stuiver and Polach, 1977). Errors on ^{14}C ages (±1σ) were based on counting statistics and $^{14}C/^{12}C$ and $^{13}C/^{12}C$ variation between data blocks. Calibration of ^{14}Cages was then performed using Marine20 calibration curve (Heaton et al., 2020) with a reservoir age (ΔR) set to 0.

2.9.5. Uranium-thorium isotope measurements

Uranium/thorium (U/Th) series were also used to constrain coral ages. The U/Th aliquots were spiked, dissolved, and separated using a chemical separation fully described in Maccali et al. (2020), largely derived from Edwards (1988). Both Th and U fractions were then analysed on a Nu Plasma II™ MC-ICP-MS at Geotop (Montreal) by peak jumping on a filtered ion counter in wet plasma mode, due to instabilities of the Aridus II™ desolvation system. Mass bias was corrected using the $^{236}U/^{233}U$ spike ratio (IRMM 3636a). Harwell uraninite (HU-1) solution was used as a standard solution to monitor analytical sessions. Activity ratios were calculated using decay constant values from Bourdon et al. (2003). Ages were calculated using the Excel Isoplot add-in 3.75 (Ludwig, 2003) without decay constant uncertainties.

2.9.6. Neodymium isotope measurements

The present study measured radiogenic neodymium isotopes (ε_{Nd}) to proxy water-mass mixing and past changes in ocean circulation concurrent with coral growth. Cleaned coral powder was dissolved in concentrated 15N nitric acid for Nd isotopes analysis. The light Rare Earth Elements (LREE) fraction was separated from other trace and major elements using an Eichrom TRU-spec® resin in diluted HNO_3, and Nd was then isolated from the other LREE using Ln-Spec® resin with diluted HCl (Pin and Zalduegui, 1997). Chemical blanks were ~300 pg for Nd, and Nd measurements were then carried out on a Nu Plasma II™ MC-ICP-MS in dry mode using an ARIDUS II™ at Geotop (Montreal). Mass fractionation was corrected using the standard exponential law with internal normalisation to $^{146}Nd/^{144}Nd$ ratio of 0.7219 (O'Nions et al., 1978). The $^{143}Nd/^{144}Nd$ ratios were calibrated against the JNdi-1 reference standard with an assigned value of 0.512115 ± 0.000007 (Tanaka et al., 2000). Nd isotopic composition is expressed as:

$$\varepsilon_{Nd} = \left\{ \left({}^{143}Nd/_{144}Nd \right)_{Sample} \Big/ \left({}^{143}Nd/_{144}Nd \right)_{CHUR} - 1 \right\} * 10^4$$

where CHUR (Chondritic Uniform Reservoir) is the present-day average Earth value ($^{143}Nd/^{144}Nd)_{CHUR} = 0.512638$ (Jacobsen and Wasserburg, 1980).

2.10. Permissions

A special permit was issued by the Bermuda Government to conduct this work (Department of Environment and Natural Resources in Hamilton, Bermuda, Permit Number 160701; see Appendix 2 in Kenchington et al., 2017). In accordance, all samples of living material, rocks, and benthic imagery were provided to the designated authorities. Permission from the Bermuda Government was also granted to the Chief Scientist (E. Kenchington) to sample Bowditch at two locations using a Van Veen grab. Grab contents were sorted at sea and sub-sampled for fossil solitary corals that were subsequently stored at −20 °C to enable geochemical analyses on shore to reconstruct the seamount's glacial history.

3. Results

3.1. Contemporary seamount water masses and connectivity to subpolar and polar regions

The first composite oceanographic section between Atlantic Canada and Bermuda, and time-depth evolutions of seawater temperature, salinity and density constructed from multiple datasets as outlined in the Methods allowed us to examine remote subpolar oceanic connections to Bowditch Seamount.

Four important layers were identified in the section plots, two of which represent distinct water masses of subpolar (LSW) and polar (Denmark Strait Overflow Water or DSOW), origin. The selection of the density contours for confining these two water masses was based on a number factors, including the history of LSW class formation and spreading, reduced potential vorticity, and elevated oxygen concentration. The LSW range used in the present study corresponds to the denser class of LSW that already reached the Bermuda domain. It is well aligned with the local oxygen maximum. The same approach was applied to defining the DSOW layer. For the thermocline density, a clear signature of this is the oxygen minimum as it acts as a barrier between the upper and deeper water.

The Halifax-Bermuda composite section (Fig. 4) revealed four distinct characteristic zones, which are distinguishable by spatial uniformity of oxygen and salinity.

A temperature-salinity plot (Fig. 5) further illustrates the range of seawater density including the LSW indicated by the 27.780 and 27.834 contours in Fig. 4.

The observations revealed four distinct zones. First, the Scotian Shelf zone/subdomain (from the coast to the shelf break, approximately 250 km along the section) contains a cool, fresh upper layer, underlain by strong thermo-, halo- and pycnoclines. The bottom water between 50 and 150 km along the section is much warmer and saltier than the upper layer, with the lack of vertical mixing due to strong stratification causing a local hypoxia.

Second, the Scotian Slope and Rise zone/subdomain (approximately 250–700 km along the section) extends from the shelf break (~250 km) to the outer edge of the continental slope (~650 km). It is characterised by elevated concentration of dissolved oxygen and patches of reduced salinity in the layer typically occupied by LSW (oxygen maximum in the 1000–2500 m depth range), and DSOW (oxygen maximum in the 2500–4500 m depth range). Overall, this zone showcases the DWBC, associated with relatively fresh well-oxygenated water masses found below 900 m deep, while the highest oxygen concentrations registered within the 900–4500 m depth range are associated with the youngest least diluted versions of LSW and DSOW found south of the Scotian Shelf. These two vertical zones of elevated oxygen concentrations can also be traced across the entire section, and notably, these oxygen maxima are directly associated with water masses of subpolar (LSW) and polar (DSOW) origins (Yashayaev and Dickson, 2008), and can be used as tracers of both.

The third zone/subdomain extending from 700 to 1000 km along the section crosses the region we identify as the Slope Water Gyre or Slope Water Sea. This zone is characterised by relative horizontal uniformity of seawater properties including salinity and dissolved oxygen, with oxygen being lower and salinity being higher in its LSW and DSOW than in the same water masses in the second zone. This homogeneity in the distribution of seawater properties reveals a closed circulation or recirculation of LSW and DSOW in the gyre (Fig. 2).

The Gulf Stream front confines the Slope Water Gyre from the south and serves as the northern boundary for the fourth subdomain stretching from the Gulf Stream to the southernmost of Bermuda's seamounts. Here in the Sargasso Sea, the waters form a warm and salty 900 m-thick upper layer (labelled for consistency as Sargasso Sea Water as both LSW and Sargasso Sea Water are formed by winter convection). The lowest oxygen concentrations within the two oxygen maxima associated with LSW and DSOW are also found in the fourth zone, the Sargasso Sea, extending from Gulf Stream to Bermuda and beyond.

The stepwise transition between the four zones (Fig. 4) is explained by the complexity of the circulation and recirculation elements spanning the upper and intermediate layers north of Bermuda. The cold slope current and underlying deep western boundary current crossing the second domain of the section are part of the direct route for the signals transfer to the region from the Labrador Sea and subpolar North Atlantic as a whole. Further offshore, in the third zone, the eastward-flowing mid-depth and deep currents recirculate LSW and DSOW toward Newfoundland, explaining the reduced LSW- and DSOW-sourced oxygen and salinity signals in the third zone. To the south of the Gulf Stream (1100 km), entering the fourth zone, there is another change in direction of the upper-layer, mid-depth and deep current, to the westward, this time. This flow in fact delivers recently renewed and ventilated water to Bermuda and its seamounts. All indicated features of the complex LSW circulation-recirculation pathways can be identified in the mid-depth circulation current map based on Argo float displacements between their profiling cycles (Fig. 2). The regional zoning of the Halifax-Bermuda section once again confirms that Fig. 2, based on the Argo float displacements at 1000 m, accurately represents the mid-depth circulation-recirculation cells responsible for transporting LSW to the Bermuda Seamounts.

The CTD measurements over Bowditch Seamount and in the area confirmed the oxygen maximum and presence of LSW at the same depths as those chosen for the benthic camera survey. The CTD profiles revealed a fluorescence maximum at about 100–130 m below the sea surface, with the MVP indicating a peak in chlorophyll about 50–60 m. This offset was likely due to the CTDs only being conducted at night so there may have been a deepening of chlorophyll at this time (Fig. 6).

3.2. Spreading time

To understand how quickly remote oceanic signals could reach the seamount fauna observed in the present study (1483–1562 m deep), we co-analysed the vertical structure of normalized temperature, salinity and density anomalies in the intermediate layer to estimate the spreading time of LSW specifically as this is the water mass that bathes the camera survey site. Fig. 7 shows two major progressive developments of LSW in the Labrador Sea in 1950–1955 and again in 1987–1995.

The first development was associated with relatively cold winters in the early 1950s (Yashayaev and Loder, 2016; Yashayaev et al., 2022; Yashayaev, 2024), with the second progression of recurrently deepening convection events falling on the period of repeatedly high NAO producing the record cold, dense, deep and voluminous LSW class (Yashayaev et al., 2022; Yashayaev, 2024). Comparably long progressions of annually-averaged temperature and salinity profiles at Bermuda (Fig. 7) also show two periods of prevailingly low values, 1959–1971 and 1999–2007 below 1,000m. The two periods with cold and fresh states around Bermuda agree with those in the Labrador Sea, given a delay of about 10 years.

3.3. Species recorded including VME indicator taxa

Observations from the 4K camera images revealed strong heterogeneity in the assembly of seamount megafauna on Bowditch. Extensive coral graveyards of Fe–Mn-coated and fossilised solitary scleractinian corals mixed with the remains of calcitic soft corals were also visually confirmed, similar to those previously reported on other seamount chains in the Sargasso Sea and western North Atlantic.

Taxonomic identification from the images produced a final list of 77 megafaunal taxa including species of Porifera, Cnidaria, Polychaeta, Mollusca, Crustacea Echinodermata, Bryozoa, Chordata, and Foraminifera (Table 1), many of which are taxa that indicate the possible occurrences of several types of VMEs.

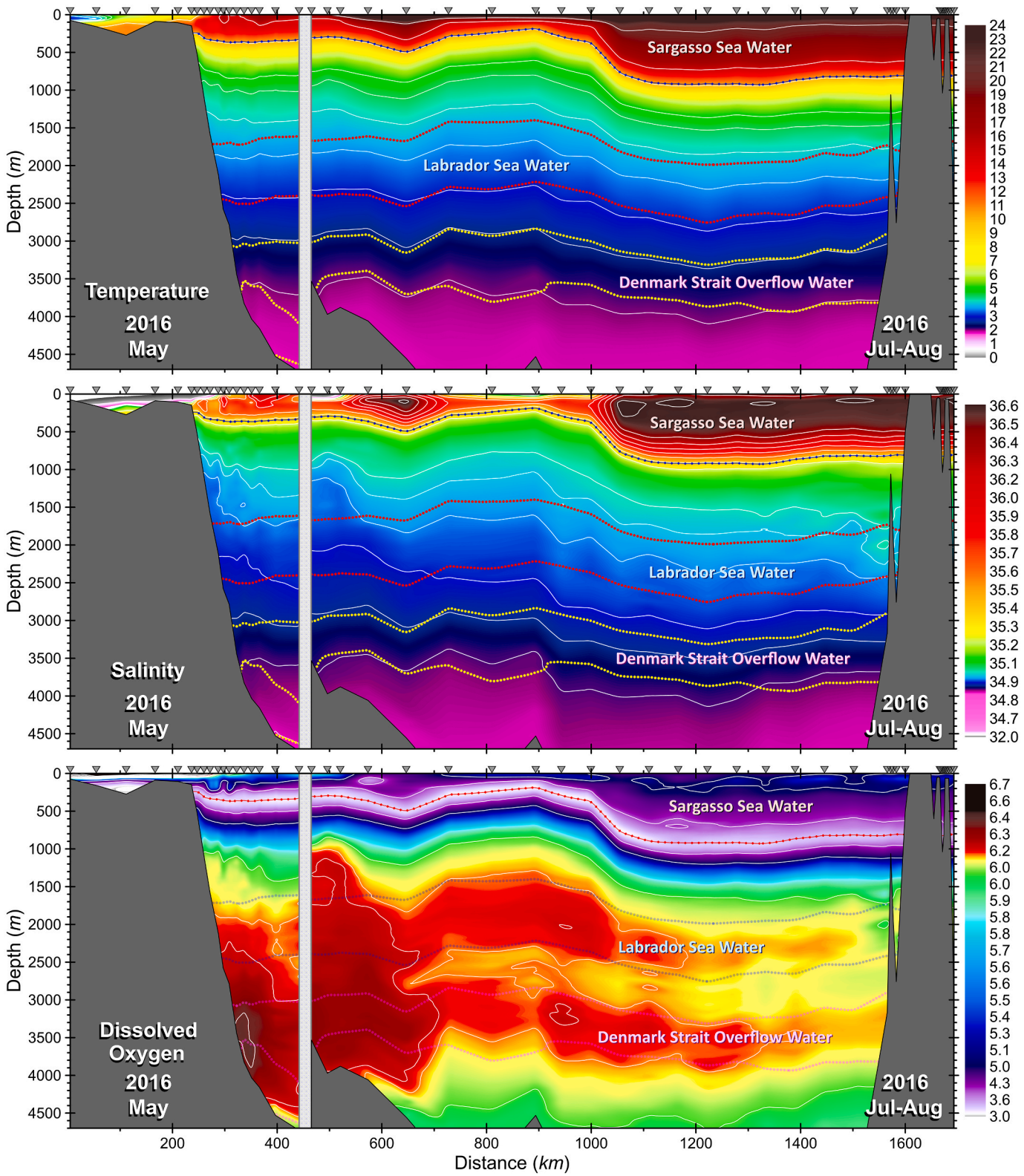

Fig. 4. Fully resolved oceanographic section from Atlantic Canada to Bermuda showing potential temperature (°C), salinity, and dissolved oxygen concentrations (ml·L^{-1}) between May–July 2016. Potential density contours are indicated by hashed lines at 27.142, 27.780, 27.834, 27.866 and 27.887 kg/m^3, with the first density contour coinciding with a strong thermocline, halocline and pycnocline, and a vertical oxygen minimum that can be traced all the way from the Scotian Slope to Bermuda's seamounts. The LSW and DSOW layers are well confined to the isopycnic layers defined by the second, third, fourth and fifth density contours.

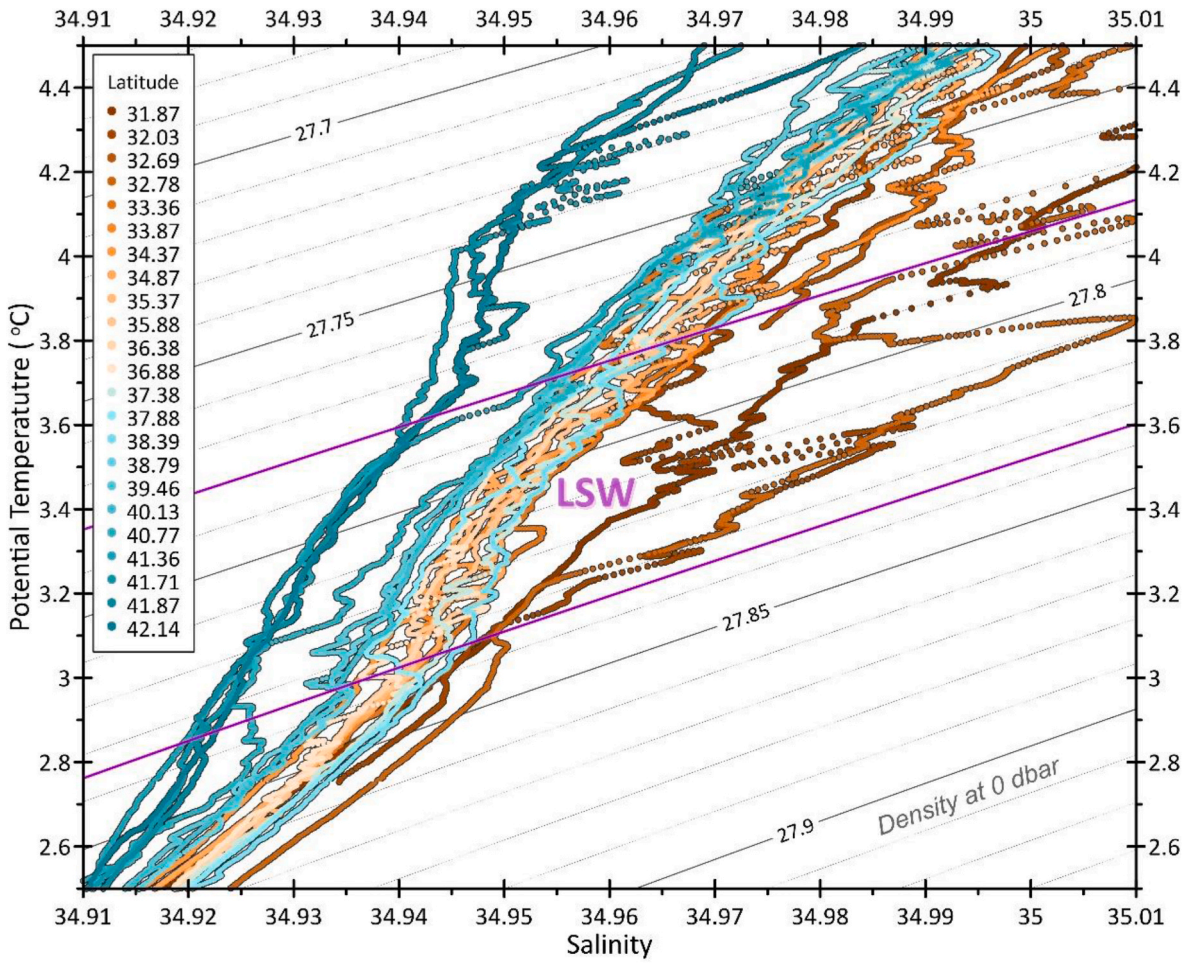

Fig. 5. Potential temperature-salinity (T–S) curves based on the full section of CTD profiles. LSW can be identified by the change in curvature of T-S curves: it tends to shoot to fresher side, but not enough to make a clear T-S minimum.

This single camera survey, 1780 m in total length, revealed: two reef framework-forming scleractinian corals (*Solenosmilia variabilis*, *Enallopsammia rostrata*), various types of coral garden-forming taxa such as black corals (*Bathypathes* sp., *Stichopathes* sp.), bamboo corals and other soft corals (e.g., *Candidella* spp., isidids, primnoids), and both glass and demosponge taxa (e.g., *Hertwigia falcifera*, cf *Farrea* sp., *Astrophorina* sp., and polymastiids). Other VME indicator taxa such as xenophyophores and stalked crinoids were also observed.

3.4. Drivers of contemporary biodiversity patterns

The total effect of all environmental variables combined on seamount biodiversity was strong and significant on Bowditch. The full RDA model explained 31% of the spatial variation in species composition (pseudo F-value = 1.887 after 500 permutations) and was statistically significant ($p < 0.0001$). Patterns in assembly or species composition were evident from visual inspection of the RDA biplot (Fig. 8).

Quantifying effects through an RDA framework enabled us to identify two major gradients relating first to larger scale spatially structured geomorphology (at scales of hundreds of metres across the camera survey transect) and second to finer scale heterogeneity in the distribution of bottom substrate type that varied at scales of several to tens of metres over the camera transect. The nearly perpendicular relationship between the spatially structured geomorphology and substrata type vector lines (Fig. 8) indicates that these were not correlated, and therefore the composition of sandy gravel, dead coral and rocky substrata varied widely over scales of several to tens of metres across the camera transect (Fig. 9).

3.4.1. Large-scale geomorphological drivers

Focussing first on larger scale drivers, northing and easting explained the largest variability or spread in species composition over the camera transect (Fig. 8). Geomorphological gradients in BPI (fine and larger scale), aspect, and plan curvature closely varied with northing and easting. Notably, the most northern and eastern camera stations tended to occur over positive topographic relief (BPI) with convex areas where currents would diverge around the relief (high values of plan curvature), with the maximum slope facing east (aspect). Conversely, stations located more to the south and west tended to be in areas with negative and more concave relief, where currents and therefore particles may converge around the seafloor surface.

RDA species scores showed more species were located in these south and west camera stations (note positive scores for RDA axis F1 in Table 1). These stations were strongly characterised (F1 values > 0, Table 1) by a rich seamount community composed of 50 species. This included VME indicator taxa such as sponges (e.g., *Hertwigia falcifera*, and a possible stalked sponge Porifera sp. 1, cf *Hyalonema* sp.), cold-water corals (e.g., *Enallopsammia rostrata*, *Bathypathes* sp., primnoids, isidiids, alcyonaceans) stalked crinoids and xenophyophores. In contrast, stations more to the north and east were strongly characterised (F1 values < 0, Table 1) by just 17 species including foraminifera, echinoids, decapods (e.g., the hermit crab Paguroidea sp.2) and Demospongiae sp. 2.

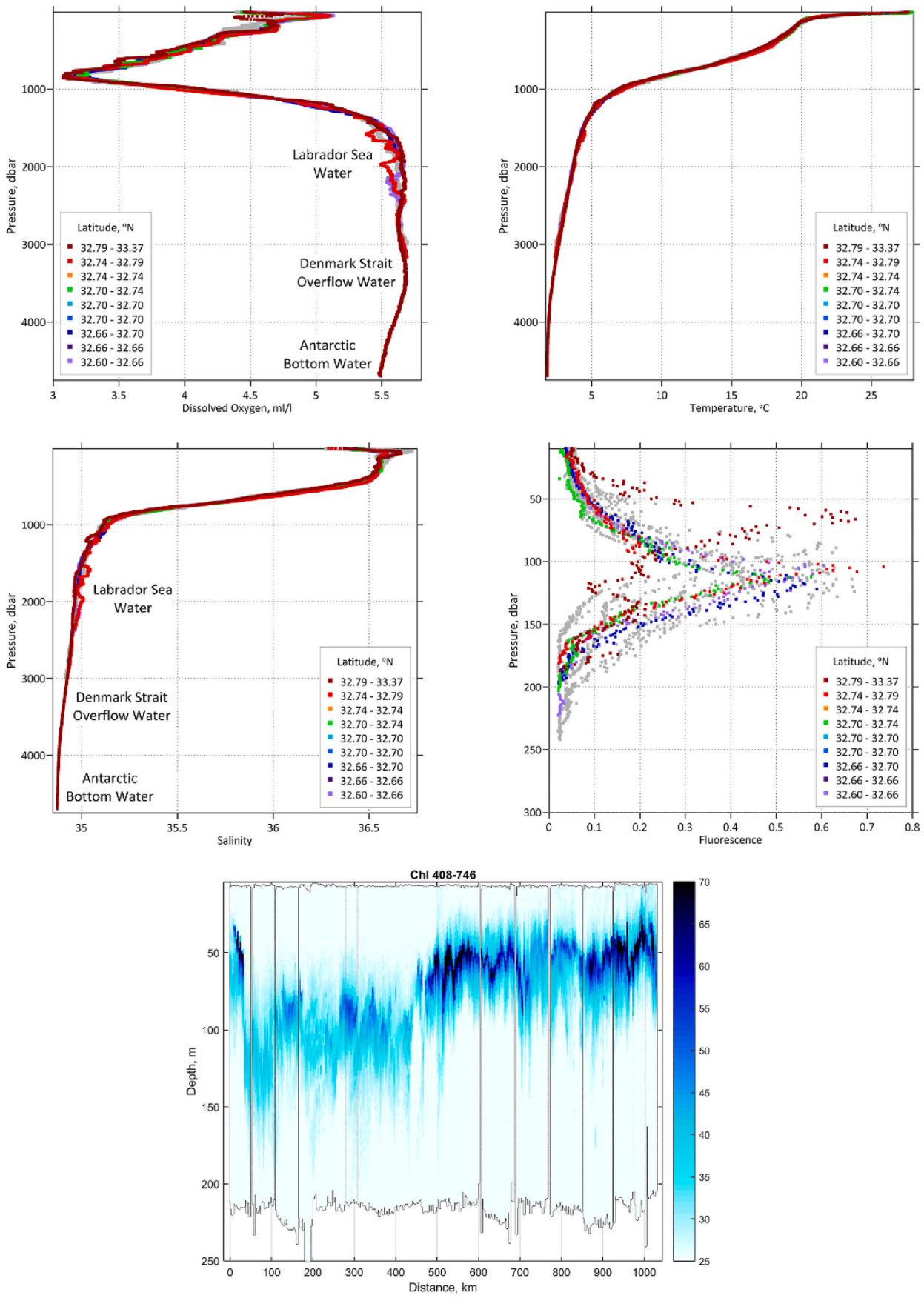

Fig. 6. Full-depth CTD profiles over and in the surroundings of Bowditch Seamount showing dissolved oxygen, potential temperature, salinity, and chlorophyll fluorescence (the latter and final bottom figure shows the MVP chlorophyll profile, with the deployment over Bowditch at 0 km).

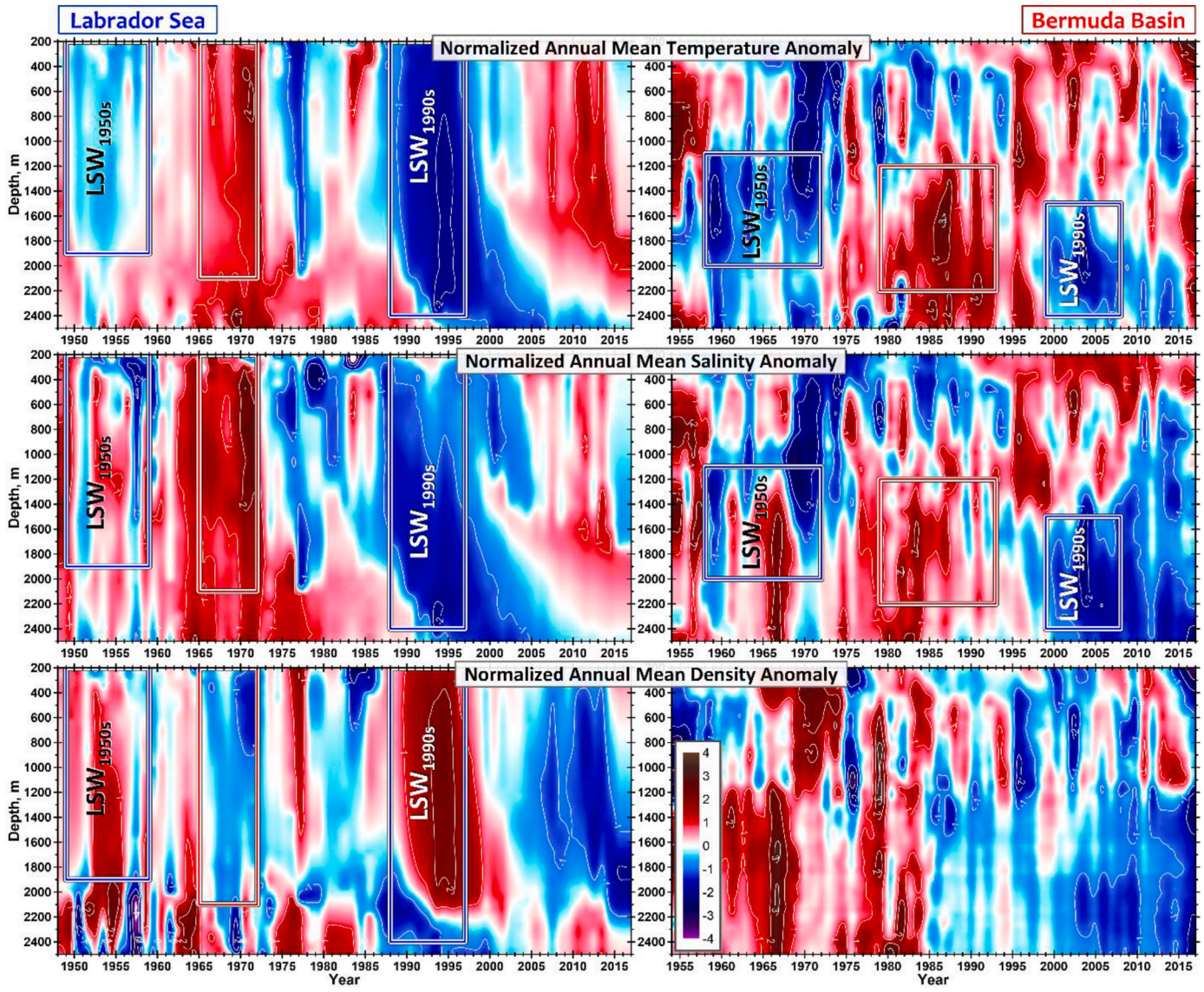

Fig. 7. Time-depth evolution and co-analysis of normalized mean potential temperature, salinity, and density anomalies in the Labrador Sea and Bermuda regions. The three rectangular-shaped boxes indicate two major cold, fresh and dense LSW state (LSW_{1950s} and LSW_{1990s}) and one warm, more saline and low-density (late 1960s) states of the intermediate layer (200–2400 m) of the Labrador Sea registered during 1948–2005, and the delayed (>10 year lagged) responses of the deep intermediate layer (1000–2400 m) at Bermuda to these events.

Thus, large-scale spatial structuring of geomorphological variables and any unmeasured spatially explicit variables are what seem to polarise the seamount fauna into a rich community to the southwest and a less species rich one to the north and west over the camera transect.

3.4.2. *Smaller scale drivers of biodiversity: substrate effects*

Focussing next on smaller-scale drivers creating heterogeneity in seamount species composition over the camera transect, the species biplot shows different substrate categories lining up closely along the second factor axis (RDA biplot axis F2, Fig. 8). Stations with high proportions of dead coral and sandy gravel were characterised by distinct communities clustered at one end of this gradient, while stations with high proportions of hard basaltic volcanic rock including outcrops were located at the opposite end of the biplot (Fig. 8).

Sandy gravel and Fe–Mn-coated dead coral were strongly characterised by just a few taxa including foraminifera. In contrast, the rocky stations were characterised by a far richer benthic community with sponges such as Porifera sp. 2, *Hertwigia falcifera*, and Demospongiae sp. 2, the latter closely resembled the carnivorous sponge genus *Cladorhiza* sp. The black coral *Stichopathes sp.* was also noted alongside a galatheid crab species (Fig. 8). A few of these rocky stations where this richer community occurred were camera stations located on extremely abrupt and steep cliffs. Notably, many VME indicator fauna that characterised these volcanic rock habitats occurred on these cliff faces and overhangs (Fig. 10).

Cliff-hanging sponges included Porifera sp. 2 and 3, *Hertwigia falcifera*, Hexactinellida sp.2 (cf *Farrea* sp.), and Demospongiae sp.1 to sp. 4. Corals on these rocky cliffs and overhangs included two black coral species *Stichopathes* sp. and *Bathypathes* sp., soft corals such as Alcyonacea sp.5, bamboo corals such as Isididae sp., three primnoid coral species Primnoidae sp. 2, *Candidella* sp. 1 (cf *gigantea*) and sp. 2, and both colonial reef framework-forming scleractinian species *Solenosmilia variabilis* and *Enallopsammia rostrata*.

3.5. *Growth history and the palaeoceanographic setting on Bowditch Seamount*

Van Veen sampling at one of the coral graveyard stations (an

Table 1
Species controlled by geomorphological gradients across the transect (RDA biplot axis F1) versus finer-scaled heterogeneity in substrate type (RDA biplot axis F2), based on absolute species scores from the redundancy analysis.

	F1	F2
Foraminifera		
Xenophyophoroidea	0.263	0.077
Foraminifera	−0.110	−0.393
Porifera		
Porifera sp.1 (possibly *Hyalonema* sp.)	0.272	−0.015
Porifera sp.2	−0.027	0.416
Porifera sp.3	0.032	0.084
Hertwigia falcifera	0.015	0.231
Hexactinellida sp.1	0.000	0.000
Hexactinellida sp.2 (possibly *Farrea* sp.)	−0.028	0.077
Polymastiidae	−0.010	−0.015
Astrophorina sp.1	0.000	0.000
Demospongiae sp.1	0.051	0.083
Demospongiae sp.2	0.264	0.882
Demospongiae sp.3	0.021	0.078
Demospongiae sp.4	0.021	0.078
Demospongiae sp.5	−0.005	−0.018
Cnidaria		
Cnidaria sp.1	0.116	−0.070
Anthozoa sp.1	0.218	−0.070
Anthozoa sp.2	0.027	−0.023
Anthozoa sp.3	0.019	−0.022
Anthozoa sp.4	−0.006	−0.021
Octocorallia sp.1	0.136	−0.078
Alcyonacea sp.1	0.532	−0.293
Alcyonacea sp.2	0.000	0.000
Alcyonacea sp.3	−0.031	−0.050
Alcyonacea sp.4	−0.017	0.006
Alcyonacea sp.5	−0.061	0.091
Alcyonacea sp.6	0.516	0.079
Isididae	0.030	0.188
Candidella sp. 1 (cf *gigantea*?)	−0.006	0.153
Primnoidae sp.1	0.038	0.001
Primnoidae sp.2	0.058	0.168
Primnoidae sp.3	0.020	−0.009
Candidella sp. 2	−0.028	0.077
Telestula sp.	0.867	−0.060
Stolonifera sp.2	0.063	−0.002
Solenosmilia variabilis	−0.008	0.069
Enallopsammia rostrata	0.058	0.168
Scleractinia sp.1	0.022	−0.007
Bathypathes sp.	0.051	0.204
Stichopathes sp.	0.184	0.492
Actiniaria sp.1	0.557	−0.331
Actiniaria sp.2	0.020	0.009
Actiniaria sp.3	0.053	0.162
Actiniaria sp.4	0.029	0.064
Corallimorpharia	0.000	0.000
Athecata sp.	0.037	0.051
Hydrozoa sp.1	0.157	0.118
Hydrozoa sp. 2	0.023	0.030
Hydrozoa sp. 3	0.013	−0.010
Bryo/Hydrozoa?	0.043	−0.009
Hydrozoa	0.023	0.030
Annelida		
Polychaeta sp.1	0.060	0.053
Polychaeta sp.2	0.024	−0.023
Mollusca		
Polyplacophora sp.	0.008	0.026
Pectinidae	0.000	0.000
Bivalvia sp.1	0.010	−0.152
Gastropoda sp.2	0.055	−0.047
Gastropoda sp.1	0.026	−0.009
Arthropoda		
Decapoda sp.1	0.006	−0.010
Decapoda sp.2	−0.031	0.009
Galatheoidea sp.1	−0.048	0.044
Galatheoidea sp.2	0.025	0.239
Paguroidea sp.1	0.016	−0.010
Paguroidea sp.2	−0.041	0.006
Echinodermata		
Comatulida	0.021	0.078
Crinoidea	0.453	−0.118
Ophiuroidea sp.1	0.051	−0.015
Ophiuroidea sp.2	0.027	−0.010
Asteroidea sp.1	0.004	−0.033
Brisingida	0.021	0.076
Echinoidea sp.1	−0.014	0.068
Echinoidea sp.2	−0.028	0.077
Bryozoa		
Bryozoa sp.1	−0.028	0.077
Bryozoa sp.2	0.023	−0.009
Chordata		
Ascidiacea sp.2	0.008	0.026
Ascidiacea sp.1	0.009	−0.018

example of which can be seen in Fig. 11) offered additional insights into the palaeoceanography and status of ancient ecosystems on Bowditch.

Coral graveyards were extensively distributed across the camera transect, indicating an ancient seamount ecosystem that favoured the proliferation of the solitary scleractinian coral *D. dianthus*. Most *Desmophyllum* skeletons yielded >95% aragonite and uranium concentrations (Table 2) were in the range expected for cold-water corals such as *D. dianthus* (≥~3.5 ppm; Smith et al., 1997; Cheng et al., 2000; Maccali et al., 2020).

Offsets of mineralogical and geochemical properties were observed in two samples (BC #3 and BC #8; Table 2) due to the mixing of isidiid coral remains (samples with bamboo corals displaying more calcitic skeletons and U-depletion; e.g., Sinclair et al., 2011) tightly attached to the aragonitic, U-enriched, *D. dianthus* skeletons.

All samples fell within two clusters of calibrated ^{14}C ages, 16.6–17.2 ka BP and ~22.6–24.7 to 25.5 ka BP (Fig. 11), with a 95.4 % probability distribution. These clusters suggest a thriving solitary scleractinian population on Bowditch Seamount slightly prior to and immediately following the LGM, likely within Heinrich Event intervals H1 and H2 (see Hemming, 2004), respectively.

Uncorrected ^{230}Th ages were not as well clustered as the ^{14}C ages (Table 2), but the two methods of age reconstruction produced broadly compatible results. The presence of ^{232}Th in all samples suggests some U and Th isotope contamination by fine detrital particles that required correction. The correction of ^{230}Th-ages is fully described in Supplementary Material S2.

The Nd isotopic composition ranged from −11.17 to −11.59, falling within the relatively radiogenic range recorded in the northwest Atlantic during the same time interval (e.g., Howe et al., 2016). The less radiogenic, sample BC#10, (−13.77) was closer to modern NADW values (Lambelet et al., 2016).

4. Discussion

Multidisciplinary analyses of the contemporary ecosystems on Bowditch Seamount revealed high numbers of VME indicators and other taxa bathed in LSW originating via remote oceanic connections to the subpolar region in the Labrador Sea convection area. Seamount benthos was structured along environmental gradients relating to large-scale changes in geomorphology and smaller scale gradients in substrate type. Parallel palaeoceanographic reconstructions of coral growth history uncovered a turbulent glacial history linked to the onsets of H2 and H1 when the Laurentide Ice Sheet discharged huge numbers of icebergs, meltwater, and vast quantities of carbonate-rich ice-rafted debris (IRD) through the Hudson Strait (Heinrich, 1988; Bond and Lotti, 1995; Hemming, 2004). Considering the modern-day context at Bowditch alongside the importance of LSW and the fossil history allows us to establish a first baseline to assess any future spatial management options, with wider consideration of how remote forcing and climate change in the subpolar regions could significantly impact seamount biodiversity in the subtropical setting of Bermuda.

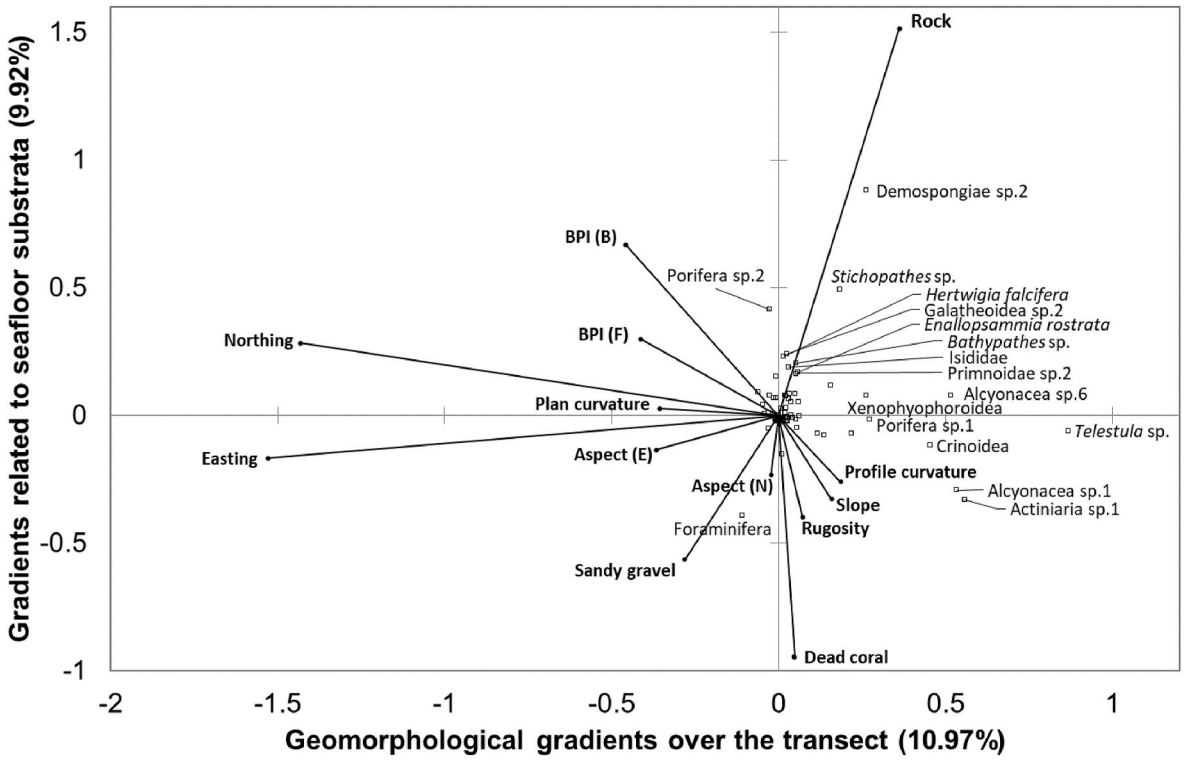

Fig. 8. RDA biplot ordination from the redundancy analysis on Bowditch, showing importance of spatially structured drivers in geomorphology (large-scale differences in seamount fauna along the first horizontal axis F1) and substrate heterogeneity (finer scale differences in seamount fauna along the second more vertical axis F2). Taxa most strongly associated with these gradients or discussed are labelled.

4.1. Water mass characteristics and remote oceanic connections

Each of the four mentioned subdomains (Shelf, Continental Slope and DWBC, Slope Water Gyre, Gulf Stream, Sargasso Sea) showed a degree of uniformity of oxygen concentration with distance along the composite section line, with step-like changes between the subdomains from high in the DWBC to low around Bermuda. The composite section also suggests that there are different circulation regimes in the four subdomains. This supports the conclusion by Chomiak et al. (2022) and our mid-depth circulation analysis that the LSW pathway from its formation to Bermuda involves large scale recirculation gyres including the Slope Water Gyre and Gulf Stream Recirculation. Both LSW and DSOW reach the outskirts of Bowditch through a complex system of currents and water-mass exchanges spanning the North Atlantic.

The time-lagged delay between two periods of progressive change between the two locations indicated a delay in LSW spreading of about 10 years required to reach Bermuda. The second of the two events reached deeper and gave record low temperature and salinity anomalies at both locations, which fully agrees with the fact that the 1987–1995 (formerly defined as 1987–1994, Yashayaev et al., 2007) LSW class was the coldest, densest, deepest, and most voluminous in the history of *in-situ* observations.

The notion that LSW spreads to Bermuda is not new, pointing at the significance of the topic for different disciplines of ocean and climate sciences. Curry et al. (1998) hypothesized that LSW reaches the Bermuda domain in about six years after its formation. However, the main signal they analysed was associated with the LSW class formed in 1987–1995 (Yashayaev et al., 2007), not allowing enough time for the coldest version of that LSW to spread to Bermuda. Additionally, the definition of LSW used in that study was static for all years and did not account for changes in LSW density between its different classes, which can overrepresent the actual water mass. These issues were resolved by Chomiak et al. (2022), who analysed longer records at four North Atlantic locations and applied class-specific definitions. Considering that the present study used a different method from Chomiak et al. (2022) to analyse seawater properties as a function of depth instead of density space, and that the present study covered a time period twice as long back to the LSW class formed in the early 1950s, the agreement between the two studies is mutually beneficial. Confirming that LSW reaches the flanks of Bermuda's seamounts 10 years after formation in the Labrador Sea, and the first synopsis of seawater properties from Atlantic Canada to Bermuda, allow more confident statements about the roles of high-latitude ocean process, deep-water ventilation and advection in food and oxygen supplies for bathyal benthic species in the subtropics. Additionally, the present time series indicated that both the cold and fresh periods and the warm and salty periods preserved their signatures when spreading downstream. These periods are defined as post-convective relaxation (Yashayaev, 2024), and such relatively short periods of declined oxygen saturation and nutrient supply may lead to severe hypoxia that could have detrimental impacts on the occurrence and survival of seamount fauna such as *D. dianthus*.

4.2. Newly documented VME indicator taxa

Annexes to the FAO International Guidelines for the Management of Deep-sea Fisheries in the High Seas document (FAO, 2009) recommend technical criteria for identifying VMEs, including through the use of indicator taxa (FAO, 2009). These groups included cold-water corals forming reefs or gardens, sponge-dominated communities, and dense emergent fauna such as crinoids and xenophyophores, hydroids and bryozoans, most of which are documented on Bowditch for the first time in the present study (Table 1). The discovery of VME indicator taxa in the present study is highly pertinent to the Bermuda government, as the Bermuda Fisheries Regulations 2010 do not permit the use of bottom trawls or dredges within the EEZ. Thus, under these regulations, the risk of significant fisheries damage to potential VMEs on Bowditch is currently low.

The present study revealed a biologically rich seamount community

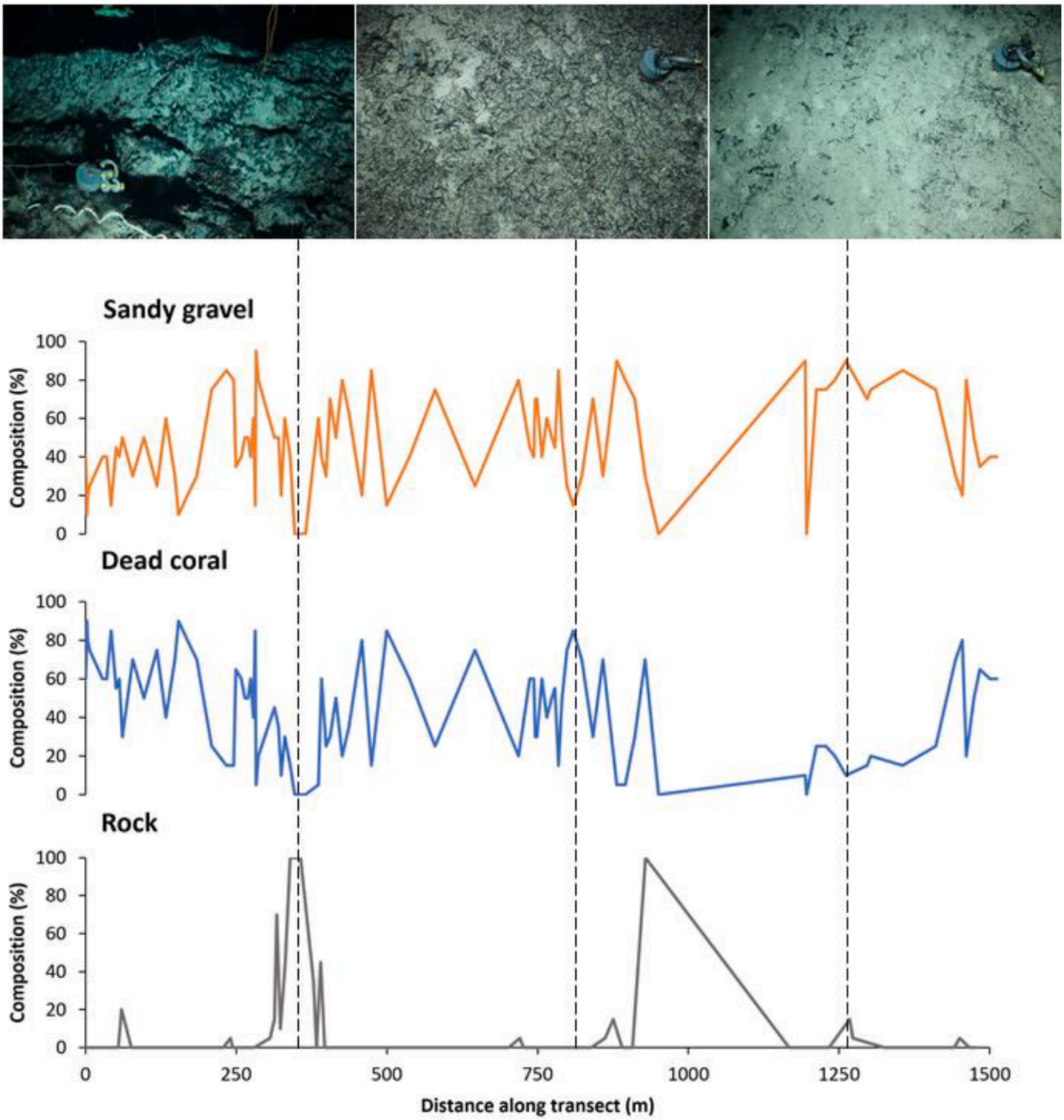

Fig. 9. Substrate classification into percent composition of sandy gravel, dead coral, and rocky seabed types over the camera transect on Bowditch Seamount. Representative images illustrate predominantly rocky, dead coral, and sandy gravel seabed types above the trend lines.

thriving in the cool, fresh, and well-oxygenated LSW layer below a chlorophyll maximum. Depending on its temporal persistence and stability, this chlorophyll maximum could also serve as a trophic subsidy mechanism that attracts visiting seamount megafauna and enhance fisheries catch (e.g., Leitner et al., 2020), but further research on this is needed at Bowditch and could support wider fisheries management in the region.

Across the camera transect, the community showed strong and significant structuring by a multitude of interacting naturally occurring environmental gradients operating at different spatial scales. This structuring adds further support to seamount research worldwide that within-seamount biological community variability can be high and is structured over multiple spatial scales (Clark et al., 2012).

The levels of endemism on Bowditch Seamount cannot immediately be determined from this study but the list of species encountered serves as the first baseline. However, Lapointe et al. (2020) found much overlap in species such as *Hertwigia* sp., *Farrea* sp., *Bathypathes* sp., *Stichopathes* spp., *Enallopsammia rostrata*, *Candidella imbricata*, primnoids,

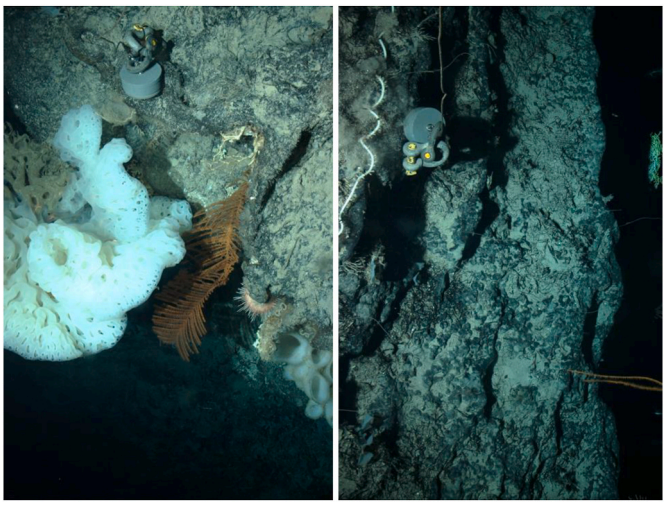

Fig. 10. Examples of cliff-hanging VME indicator fauna that characterised exposed volcanic rock on Bowditch Seamount including the hexactinellid sponge *Hertwigia falcifera* and the antipatharian black coral *Bathypathes* sp. (left panel), and a mixed coral garden assemblage of an isidid bamboo coral, the antipatharian black coral *Stichopathes* sp. and the reef-framework forming scleractinian *Enallopsammia rostrata* (right panel). Note the 4K dropframe camera's lead disc in each image (diameter for scale is 10 cm).

etc. between the neighbouring New England and Corner Rise seamounts. It's also thought that both antipatharian and octocoral taxa on these seamounts are more generally not restricted to individual seamounts (Thoma et al., 2009), but Cho and Shank (2010) revealed significant levels of genetic differentiation in seamount ophiuroids according to water depth and region along the New England, Corner Rise Seamount chains and Muir Seamount.

Our new fully resolved oceanographic sections, time-depth evolution and co-analysis concur with the concept of oceanic connections via LSW potentially providing deep biophysical connections along its bathyal pathway from its subpolar origins to Bermuda's seamounts. Cairns and Chapman (2001) found that the deep-water Scleractinia around Bermuda clustered within a greater western Atlantic supercluster and had no distinctive endemic species, being characterised primarily by amphi-Atlantic and cosmopolitan taxa, all suggesting a highly connected fauna. Future studies that integrate genetic sampling and biophysical modelling are better placed to resolve the question of seamount species endemism.

On the subject of endemism, larval dispersal on Bowditch might be constrained by seamount hydrographic features. This can include even temporary ones such as Taylor columns, tidally rectified circulation cells, and mesoscale eddy dipoles such as those found on the Maud Rise seamount (Beeston et al., 2018), Fieberling Guyot (Mullineau and Mills, 1997), and the MAD-Ridge Seamount (Vianello et al., 2020), respectively. Validating whether an upwelling and retention feature exists over Bowditch Seamount and whether it causes any cryptic variation or species endemism would require detailed molecular analyses and high-resolution hydrographic surveys over a much wider area.

4.3. Drivers of seamount fauna assembly

Larger scale spatially structured geomorphological variables controlled species composition over hundreds of metres across the camera survey on Bowditch. VME indicator taxa in particular were more prevalent in the southwestern region of this camera survey than in the northeastern part. These included many suspension-feeding VME indicator taxa including reef framework-forming scleractinians, sponges, crinoids, and bamboo corals, which could indicate potential coral gardens, crinoid or deep-sea sponge aggregations for example.

The southwestern camera stations were characterised by negative bathymetric relief and more concave areas. Negative values of plan curvature indicate that these areas of seafloor depressions are likely to be areas where currents may converge. This has implications for particle transport because these areas may be where food and sediment particles converge and are most abundant (Wilson et al., 2007) to support this biologically rich community of sessile suspension-feeding fauna, many

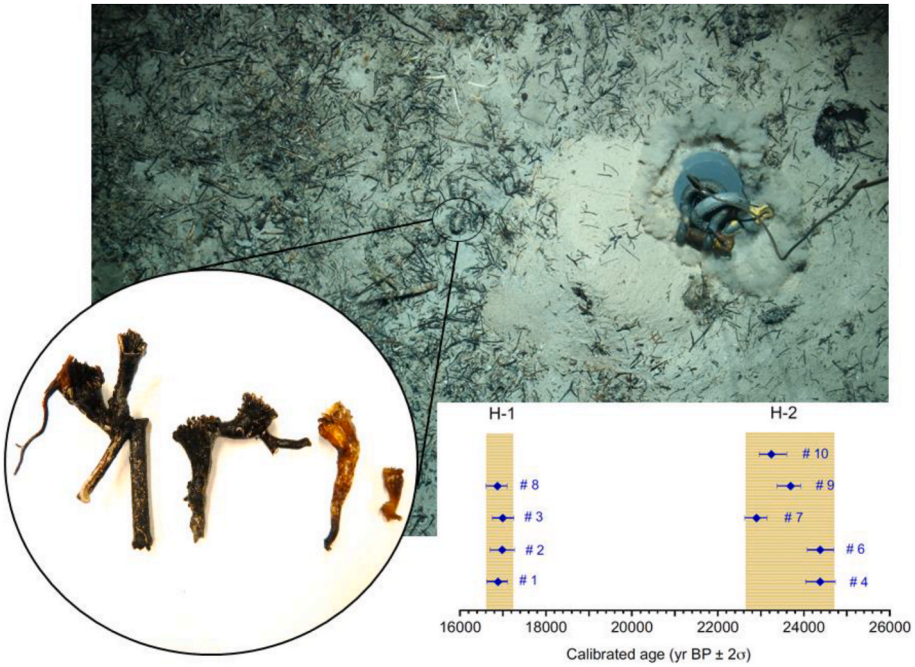

Fig. 11. Reconstruction of the fossil history on Bowditch over the last glacial maximum (LGM). An example image (CON173_047) shows a fossil graveyard with Fe–Mn-coated scleractinians and calcitic bamboo corals, amongst living white *Telestula* sp. octocorals. This type of habitat was where nine fragments of *Desmophyllum dianthus* corals were sampled by Van Veen grab (inset). The 95.4% probability distribution of calibrated ^{14}C-ages of *D. dianthus* samples is shown (inset, with ages in cal yr BP).

Table 2
Mineralogy, $^{13}C/^{12}C$ and $^{143}Nd/^{142}Nd$ compositions, U-series and radiocarbon ages of *D. dianthus* samples. ^{14}C-ages are calibrated using Calib 8.2 (Stuiver and Reimer, 1993) and the Marine20 calibration curve (Heaton et al., 2020) with a ΔR set to 0, with 95.4% probability; [2]Corrected ^{230}Th-ages are calculated using an initial ($^{230}Th/^{232}Th$) activity ratio of 17 from station 10 of the GA03 GEOTRACES transect in the area (see Supplementary Material S2 for details).

Sample number	Aragonite (%)	Calcite (%)	^{14}C age ± 1σ (yr BP)	(1)Medium calibrated ^{14}C age (BP)	Uncorr. ^{230}Th age (ka) ± 2σ	(2)Corr. ^{230}Th ages (ka) ± 2σ	$\delta^{13}C$ ± 1σ	ε_{Nd} ± 2σ
BC 1	98.5	1.5	14,629 ± 47	16,886	16.81 ± 0.14	16.62 ± 0.14	−4.13 ± 0.01	−11.17 ± 0.33
BC 2			14,711 ± 73	16,984				
BC 3	21.3	78.7	14,720 ± 43	16,995	18.77 ± 0.18	17.69 ± 0.17	−2.24 ± 0.01	
BC3 duplicate					18.57 ± 0.30	17.58 ± 0.22		
BC 4			21,121 ± 72	24,380				
BC 6	99.1	0.9	21,028 ± 92	24,379	24.29 ± 0.37	23.96 ± 0.21	−5.60 ± 0.01	−11.59 ± 0.23
BC 7			19,794 ± 67	23,348				
BC 8	3.6	96.4	14,617 ± 49	16,872	21.34 ± 2.28	21.40 ± 2.60	0.44 ± 0.01	
BC 9	95.5	4.5	20,494 ± 74	23,691	24.40 ± 0.28	24.17 ± 0.26	−6.00 ± 0.01	−11.56 ± 0.35
BC 10	99.3	0.7	20,110 ± 75	23,245	24.48 ± 0.42	24.11 ± 0.27	−5.48 ± 0.01	−13.77 ± 0.20

of which are also VME indicator taxa. Future investigations could deploy sediment traps and acoustic Doppler current profiles to complement these geomorphological proxies with ground-truthed measurements of sediment transport in these areas.

Smaller scale heterogeneity in bottom substrate type (at scales of several metres within smaller patches on the seamount) was almost as strong a driver of within seamount variability as geomorphology, and a significant factor as reported on other seamounts (Henry et al., 2014; Du Preez et al., 2016; Morgan et al., 2019). At Bowditch Seamount, camera sites from fossil coral graveyards had predominantly more gravelly sediments and notably the profile curvature was also positive, indicating areas of the seafloor where currents might decelerate. These stations were characterised by far fewer species more specialised to live on unconsolidated sediments such as some foraminiferans including dense aggregations of a xenophyophore species, a possible VME indicator. Xenophyophores can dominate large swathes on a single seamount and can significantly modify adjacent benthic communities by enhancing the local biodiversity of infaunal communities (Levin and Thomas, 1988). Recently they have also been shown to be nurseries for liparids (snailfishes) who deposit eggs in the xenophyophore tests (Levin and Rouse, 2019).

In contrast, many other taxa including VME indicators peaked on exposed volcanic rocky outcrops with negative profile curvature where currents might decelerate. These stations were occupied by large suspension-feeding cold-water corals including reef framework-forming corals *Solenosmilia variabilis*, *Enallopsammia rostrata* and at least two black coral species, *Bathypathes* sp. and *Stichopathes* sp. Very similar occurrences of both scleractinian and antipatharian corals have been noted in the northeastern Atlantic on exposed bedrock portions of Hatton Bank (Roberts et al., 2008) and on glacial dropstones in the vicinity of coral carbonate mounds on Rockall Bank (De Clippele et al., 2019). Although no measurements of local current speeds or particles were obtained during the present study, future investigations could test the hypothesis that food supply to these sessile suspension feeders on rocky substrata are supported by decelerated flow, which on the larger scale, would relate to gradients in seafloor concavity to the south west along this camera transect.

4.4. Coral growth history at bowditch seamount

Desmophyllum skeleton aragonite and uranium concentrations were in the range expected for cold-water corals such as *D. dianthus* (≥~3.5 ppm; Smith et al., 1997; Cheng et al., 2000; Maccali et al., 2020). The ^{14}C-calibrated ages broadly concurred with the U-series ages. Together, these paired geochemical analyses helped identify two intervals of *D. dianthus* occurrences on Bowditch Seamount: the first being a millennial-duration growth interval slightly preceding the LGM, and the second being a shorter centennial-duration interval immediately following the LGM. These ages concur with growth histories at nearby Muir Seamount and the New England Seamount Chain (Robinson et al., 2007; Thiagarajan et al., 2013).

The widely scattered ^{14}C-calibrated ages prior to the LGM are notable and could be related to large amplitude variations in ventilation ages of ambient waters. This growth interval overlaps Heinrich Event 2 (H2) at ~24 ka (Hemming, 2004), a time characterised by significant changes in deep and surface ocean conditions. During the peak of the LGM, Bowditch might have still been at the core of a shallow, well-ventilated cell of the North Atlantic (Freeman et al., 2016). Corrected ^{230}Th-ages of three samples from the pre-LGM interval (BC#6, BC #9, and BC #10; Table 2) depicted a very narrow age range (24.39 ± 0.09 ka; ±1σ) in contrast to their calibrated ^{14}C-ages (24.0 ± 0.4 ka; ±1σ). This would support the theory that corals growing on Bowditch Seamount could have experienced large changes in ^{14}C-ventilation ages of the ambient water mass during Heinrich event 2. However, the small number of samples and the complex correction of ^{230}Th-ages prevented a firmer conclusion in the present study.

Neodymium isotopic compositions indicate that proxies of water mass composition and mixing were within ranges reported for the same intervals in the western North Atlantic (Howe et al., 2016; Lambelet et al., 2016). Our values do suggest a more radiogenic water source, perhaps the Glacial North Atlantic Intermediate Water (GNAIW), during coral growth intervals. These values contrast with the modern NADW mass, which has a substantial LSW contribution in its upper layer. A less radiogenic value ($\varepsilon_{Nd} = -13.8 \pm 0.2$) was recorded by one sample (BC #10), dated ~ 23,245 ± 300 BP (^{14}C-calibrated; Table 2). It falls within other values reported for the modern NADW, which is strongly influenced by the low-radiogenic supplies from LSW (e.g., Lambelet et al., 2016). Compared with the ~1 ka-older sample #6 value ($\varepsilon_{Nd} = -11.6 \pm 0.2$), it indicates substantial short-term variability in the water mass dynamics just prior to the LGM. This coral age range (~23.8–~24.7 ka) encompasses H2 dated ~ 24 ka (Hemming, 2004), an interval marked by the release of huge amounts of ice-rafted unradiogenic pre-Cambrian material in the North Atlantic (e.g., Andrews et al., 1996). Thus, the outlier ε_{Nd}-value of sample BC #10 could simply be linked to this event, as LSW convection did not begin until about 7000 years ago (Hillaire-Marcel et al., 2001).

Returning to the pre- and post-LGM growth history at Bowditch, the fact that both coral growth episodes match Heinrich events triggered in the Hudson Strait with detrital sedimentary sources containing abundant detrital carbonates (Hillaire-Marcel et al., 1994; Andrews et al.,

1994, 1996; Hemming, 2004) was notable. The pre-LGM samples (Heinrich event 2, H-2) showed a scatter of ages, either due to optimal coral growth over a long-duration carbonate event or to changes in the ^{14}C-ventilation age of ambient water mass throughout this event.

In both cases, it seems likely that ice-rafting debris (IRD) resulted in a strong buffering of the water column with a resulting deepening of the aragonite compensation depth, a critical element for the growth of post-glacial *D. dianthus* found at slightly greater depths in the Labrador Sea (Maccali et al., 2020). Coral growth during H2 and H1 ages coincided with intervals when IRD of carbonates likely resulted in a lower aragonite compensation depth, which seems likely to best explain the "boom and bust" phenomena of *D. dianthus* on other seamounts in the Northwest Atlantic (Thiagarajan et al., 2013).

Alternative and not mutually exclusive hypotheses for the boom-and-bust phenomena in western North Atlantic *Desmophyllum dianthus* populations are other inter-related factors: changes in food supply and productivity, altered physicochemical and hydrographical settings in oxygen concentration and aragonite saturation (Thiagarajan et al., 2013; Maccali et al., 2020) but also stratification and mixing.

4.4.1. Food theories

The conspicuous absence of solitary corals in the contemporary bathymetric setting of Bowditch Seamount precisely corresponds with modern-day observations from the New England Seamount Chain where modern *D. dianthus* were also largely absent at the same water depths (Robinson et al., 2007; Thiagarajan et al., 2013). Further north on Orphan Knoll in the Labrador Sea, primary productivity based on coccolithophorids is thought to have contributed to the particulate and dissolved organic carbon diet of the corals (Maccali et al., 2020). Today in this region, slope and orientation (and thus effects of prevailing currents) are found to have a strong influence on the modern-day distribution of *D. dianthus* (Meredyk, 2017), which suggests a possibly strong driver of food supply on its occurrence.

If we examine the physiological and feeding niche of *Desmophyllum dianthus* more closely, then it becomes apparent how sensitive this species might be to shifts in food supply. The species is a generalist zooplankton predator capable of consuming prey over a wide size range including copepods and euphasiids (Höfer et al., 2018). This species also feeds on suspended particulate organic matter (POM) derived from sinking POM (Wang et al., 2014). Conditions marked by lower pH and reduced aragonite saturation combined with lower prey or POM availability can therefore cause significant mortality rates and result in slower calcification rates (Martínez-Dios et al., 2020).

Around ~17.5 ka calendar age BP, an increase in wind-driven upwelling and concentrations of silicic acid in the thermocline caused widespread diatom blooms and silicon utilisation across the Sargasso Sea (Hendry et al., 2014). This could have substantially increased the export of biological production due to a rapid sinking of material out of the surface ocean, and fuelled a *D. dianthus* boom on Bowditch Seamount at that time. In modern times however, Henson et al. (2012) found that most exported organic carbon likely gets rapidly remineralised in the euphotic zones of low latitude regions. This appears to be the case at the Bermuda Atlantic Time-series study (BATS) station, where transfer efficiency to the mesopelagic zone is lower due to the effect of warmer temperatures on POC remineralisation (DeVries and Weber, 2017). Deglacial trends in remineralisation rates could be investigated to further test this hypothesis.

Notably, stable isotopes from the present study were within the range commonly observed in deep-sea corals. Low δ^{13}C values (linked to physiological oxidation of organic matter and release of ^{13}C-depleted CO_2) were observed in most samples except for BC #8 (Table 2), where most of the material recovered was likely from the intimately mixed bamboo coral. Scleractininan corals either have a drastically distinct metabolism from their octocoral counterparts on Bowditch, or some important contribution of coccolithophorids in bamboo coral diet could explain the relative enrichment in δ^{13}C in BC #8 (e.g., Ziveri et al., 2003; Saenger et al., 2017).

4.4.2. Oxygen and ventilation theories

Changes in ocean ventilation rates and oxygen concentration are expected in an era of rapid climate change (Shepherd et al., 2017). This is due to effects of increased stratification on ocean circulation and ventilation, e.g., due to reduced upwelling, deep-water formation and turbulent mixing. Because O_2 solubility decreases at higher water temperatures, this will reduce oxygen concentration as will the effects of warming on biological production, respiration, and remineralisation (Shepherd et al., 2017).

The water mass bathing the seamount during the deglacial around 18 kyr BP, possibly GNAIW, may have had reduced nutrients (Lynch-Stieglitz et al., 2014) but it may have also been more radiogenic than the modern NADW as a result of reduced LSW contributions (Gutjahr et al., 2008). Jaccard and Galbraith (2012) and Bopp et al. (2017) agreed that the upper 1500 m of the ocean became deoxygenated over the deglaciation. The combination of warming-induced decreases in O_2 concentrations and increasing apparent oxygen utilisation (AOU) might have been driven by reduced water mass ventilation ages and caused this decline (Bopp et al., 2017). Corrected ^{230}Th-ages of pre-LGM corals versus their calibrated ^{14}C-ages (~24.0 ± 0.3 ka; ±1σ) support the theory that corals experienced large changes in ocean ventilation prior to the LGM, but not during the deglacial interval of coral growth.

5. Conclusions

This first baseline assessment of environmental controls on Bowditch Seamount's benthic communities, past and present, and oceanographic connections to the Labrador Sea provide new data on the occurrence of VME indicator taxa around Bermuda and suggests potential sensitivities to properties and dynamics of distant forcing factors originating in subpolar and polar regions. Today, the seamount community is bathed by an oxygen-rich LSW layer. However, the LSW alternates between warm more saline states and cooler fresher states, with the implications on the seamount fauna we studied not being known. Furthermore, the seamount's fossil history indicates a turbulent past and ecosystem reorganisation that could relate to the food availability and/or aragonite compensation depth. This further suggests that climatic variability in LSW properties and dynamics could dramatically shift the community to a new baseline, and we now know this could spread to the seamount in 10 years or less.

CRediT authorship contribution statement

Lea-Anne Henry: Writing – review & editing, Writing – original draft, Visualization, Validation, Supervision, Software, Resources, Project administration, Methodology, Investigation, Funding acquisition, Formal analysis, Data curation, Conceptualization. **Igor Yashayaev:** Writing – review & editing, Writing – original draft, Visualization, Validation, Supervision, Software, Resources, Project administration, Methodology, Investigation, Funding acquisition, Formal analysis, Data curation, Conceptualization. **Claude Hillaire-Marcel:** Writing – original draft, Visualization, Validation, Supervision, Software, Resources, Project administration, Methodology, Investigation, Funding acquisition, Formal analysis, Data curation, Conceptualization. **F. Javier Murillo:** Writing – review & editing, Writing – original draft, Visualization, Validation, Supervision, Software, Resources, Project administration, Methodology, Investigation, Funding acquisition, Formal analysis, Data curation, Conceptualization. **Ellen Kenchington:** Writing – review & editing, Writing – original draft, Visualization, Validation, Supervision, Software, Resources, Project administration, Methodology, Investigation, Funding acquisition, Formal analysis, Data curation, Conceptualization. **Struan Smith:** Writing – review & editing, Writing – original draft, Visualization, Validation, Supervision, Software, Resources, Project administration, Methodology, Investigation,

Funding acquisition, Formal analysis, Data curation, Conceptualization. **Jenny Maccali:** Writing – review & editing, Writing – original draft, Visualization, Validation, Supervision, Software, Resources, Project administration, Methodology, Investigation, Funding acquisition, Formal analysis, Data curation, Conceptualization. **Jill Bourque:** Writing – review & editing, Writing – original draft, Visualization, Validation, Supervision, Software, Resources, Project administration, Methodology, Investigation, Funding acquisition, Formal analysis, Data curation, Conceptualization. **Louis L. Whitcomb:** Writing – review & editing, Writing – original draft, Visualization, Validation, Supervision, Software, Resources, Project administration, Methodology, Investigation, Funding acquisition, Formal analysis, Data curation, Conceptualization. **J. Murray Roberts:** Writing – review & editing, Writing – original draft, Visualization, Validation, Supervision, Software, Resources, Project administration, Methodology, Investigation, Funding acquisition, Formal analysis, Data curation, Conceptualization.

Declaration of competing interest

The authors declare that they have no known competing financial interests or personal relationships that could have appeared to influence the work reported in this paper.

Data availability

Data will be made available on request.

Acknowledgements

We gratefully acknowledge the support of the captain and crews (Coast Guard and scientific) of the CCGS *Hudson* during the HUD2016006 hydrographic cruise and the HUD2016019 *International Deep Sea Science Expedition*. We would like to thank Dan Hut with Defence Research and Development Canada (DRDC) for their contribution of an MVP 200 (Moving Vessel Profiler) and operators Daniel Graham, and Mark Fotheringham. We thank the Canadian Hydrographic Service; Joe Manning, Jonathan Griffin and David Levy for providing the fish, topside unit (MVO controller Interface and DTM) and sensors (sound velocity and CTD); George States and Jason Greene (DFO) who provided sensors (CTD and fluorometer) as well as technical support, and Natural Resources Canada (NRCan) for technical support and the use of their benthic sampling gear. We would also like to thank the Bermuda Government for their support and assistance during the HUD2016019 expedition. Finally, we would like to thank Neil MacKinnon (DFO) for Logistic support. Camille Lirette, Barry MacDonald both of Fisheries and Oceans Canada (DFO) were instrumental to the procurement of the data used in this publication. We thank Yang Zhang (the University of Delaware) for constructing the map of ocean currents in the Bermuda region based on ECCO re-analysis. Canadian participation in the expedition was funded by a DFO International Governance Strategy project awarded to EK, while ship time was provided by DFO. This project has received funding from the European Union's Horizon 2020 research and innovation programme under grant agreements No. 678760 (ATLAS), No. 679849–2 (SponGES) and No. 818123 (iAtlantic), as well as from the *Fonds Québécois de Recherche (Nature et technologies)* for the partial funding of analytical work at Geotop. Whitcomb acknowledges the support of the U.S. National Science Foundation under awards OCE-1435818 and IIS-1909182. This output reflects only the authors' views and the European Union cannot be held responsible for any use that may be made of the information contained therein. The views and conclusions in this article represent the views of the U.S. Geological Survey. Any use of trade, product, or firm names is for descriptive purposes only and does not imply endorsement by the US Government.

Appendix A. Supplementary data

Supplementary data to this article can be found online at https://doi.org/10.1016/j.dsr.2024.104342.

References

Addy, S.K., 1979. Rare earth element patterns in manganese nodules and micronodules from northwest Atlantic. Geochem. Cosmochim. Acta 43, 1105–1115.
Adkins, J., 2003. New England seamounts. AT7-35 Medusa Cruise Report 85.
Adkins, J.F., Henderson, G.M., Wang, S.-L., O'Shea, S., Mokadem, F., 2004. Growth rates of the deep-sea scleractinia *Desophyllum cristigalli* and *Enallopsammia rostrata*. Earth Planet Sci. Lett. 227, 481–490.
Andrews, J.T., Bergsten, B., Jennings, A.E., 1996. Late quaternary palaeoceanography of the North atlantic margins. Geological Society Special publication 111, 376.
Andrews, J.T., Tedesco, K., Briggs, W.M., Evans, L.W., 1994. Sediments, sedimentation rates, and environments, SE baffin shelf and NW Labrador Sea 8 to 26 ka. Can. J. Earth Sci. 31, 90–103.
Auscavitch, S.R., Deere, M.C., Keller, A.G., Rotjan, R.D., Shank, T.M., Cordes, E.E., 2020. Oceanographic drivers of deep-sea coral species distribution and community assembly on seamounts, islands, atolls, and reefs within the Phoenix Islands Protected Area. Front. Mar. Sci. 7, 42.
Bates, N.R., Best, M.H.P., Neely, K., Garley, R., Dickson, A.G., Johnson, R.J., 2012. Detecting anthropogenic carbon dioxide uptake and ocean acidification in the North Atlantic Ocean. Biogeosciences 9, 2509–2522.
Bates, N.R., 2017. Twenty years of marine carbon cycle observations at Devils Hole Bermuda provide insights into seasonal hypoxia, coral reef calcification, and ocean acidification. Front. Mar. Sci. 4, 36.
Beazley, L.I., Kenchington, E.L., Murillo, F.J., Sacau, M., 2013. Deep-sea sponge grounds enhance diversity and abundance of epibenthic megafauna in the Northwest Atlantic. ICES (Int. Counc. Explor. Sea) J. Mar. Sci. 70, 1471–1490.
Beeston, M.A., Cragg, S.M., Linse, K., 2018. Hydrological features above a Southern Ocean seamount inhibit larval dispersal and promote speciation: evidence from the bathyal mytilid *Dacrydium alleni* sp. nov. (Mytilidae: Bivalvia). Polar Biol. 41, 1493–1504.
Berkowitz, Z., Fujii, J., Vaughn, I., Vaccaro, J., Belani, M., Cole, A., 2018. *Sentry* Operations Report for the AE1823 Kinsey Cruise (DRAFT). WHOI Sentry Operations Group, Woods Hole Oceanographic Institution, 2018.
Bond, G.C., Lotti, R., 1995. Iceberg discharges into the North Atlantic on millennial time scales during the last glaciation. Science 267, 1005–1010.
Bopp, L., Resplandy, L., Untersee, A., Le Mezo, P., Kageyama, M., 2017. Ocean (de) oxygenation from the Last Glacial Maximum to the twenty-first century: insights from Earth System models. Philosophical Transactions of the Royal Society A 375, 20160323.
Boschen, R.E., Rowden, A.A., Clark, M.R., Barton, S.J., Pallentin, A., Gardner, J.P.A., 2015. Megabenthic assemblage structure on three New Zealand seamounts: implications for seafloor massive sulfide mining. Mar. Ecol. Prog. Ser. 523, 1–14.
Bourdon, B., Turner, S., Henderson, G.M., Lundstrom, C.C., 2003. Introduction to U-series geochemistry. Rev. Mineral. Geochem. 52, 1–21.
Cairns, S.D., Chapman, R.E., 2001. Biogeographic affinities of the North atlantic deep-water scleractinia. In: Proceedings of the First International Symposium on Deep-Sea Corals, Ecology Action Centre and Nova Scotia Museum, pp. 30–56. Halifax, Nova Scotia, Canada.
Calder, D.R., 1998. Hydroid diversity and species composition along a gradient from shallow waters to deep sea around Bermuda. Deep-Sea Res. Part I 45, 1843–1860.
Calder, D.R., 2000. Assemblages of hydroids (Cnidaria) from three seamounts near Bermuda in the western North Atlantic. Deep Sea Res. Oceanogr. Res. Pap. 47, 1125–1139.
Canache, C., 2007. Fishes of the new England seamounts. In: Undergraduate Thesis. Wilkes Honours College, Florida Atlantic College, p. 28.
Cheng, H., Adkins, J., Edwards, R.L., Boyle, E.A., 2000. U-Th dating of deep-sea corals. Geochem. Cosmochim. Acta 64, 2401–2416.
Cho, W.W., 2008. Faunal Biogeography, Community Structure, and Genetic Connectivity of North Atlantic Seamounts. Ph.D. Thesis, p. 181. MIT/WHOI, 2008-15.
Cho, W.W., Shank, T.M., 2010. Incongruent patterns of genetic connectivity among four ophiuroid species with differing coral host specificity on North Atlantic seamounts. Mar. Ecol. 31 (s1), 121–143.
Chomiak, L.N., Yashayaev, I., Volkov, D.L., Schmid, C., Hooper, J.A., 2022. Inferring advective timescales and overturning pathways of the deep western boundary current in the North atlantic through Labrador Sea Water advection. J. Geophys. Res.: Oceans 127, e2022JC018892.
Clark, M.R., Bernardino, A.F., Roberts, J.M., Narayanaswamy, B.E., Snelgrove, P., Tuhumwire, J.T., 2021. Seamounts and Pinnacles. The 2nd World Ocean Assessment (Volume 1, Chapter 7L). United Nations, pp. 437–451.
Clark, M.R., Bowden, D.A., 2015. Seamount biodiversity: high variability both within and between seamounts in the Ross Sea region of Antarctica. Hydrobiologia 761, 161–180.
Clark, M.R., Bowden, D.A., Rowden, A.A., Stewart, R., 2019. Little evidence of benthic community resilience to bottom trawling on seamounts after 15 years. Front. Mar. Sci. 6, 63.
Clark, M.R., Schlacher, T.A., Rowden, A.A., Stocks, K.I., Consalvey, M., 2012. Science priorities for seamounts: research links to conservation and management. PLoS One 7, e29232.

Coates, K.A., Fourqurean, J.W., Kenworthy, W.J., Logan, A., Manuel, S.A., Smith, S.R., 2013. In: Sheppard, C.R.C. (Ed.), Coral Reefs of the United Kingdom Overseas Territories, Coral Reefs of the World 4, pp. 115–133.
Coplen, T.B., 1996. New guidelines for reporting stable hydrogen, carbon, and oxygen isotope-ratio data. Geochem. Cosmochim. Acta 60, 3359–3360.
Coplen, T.B., Brand, W.A., Gehre, M., Gröning, M., Meijer, H.A.J., Toman, B., Verkouteren, R.M., 2006. After two decades a second anchor for the VPDB $\delta^{13}C$ scale. Rapid Commun. Mass Spectrom. 20, 3165–3166.
Crann, C.A., Murseli, S., St-Jean, G., Zhao, X., Clark, I.D., Kieser, W.E., 2017. First status report on radiocarbon sample preparation techniques at the AE Lalonde AMS Laboratory (Ottawa, Canada). Radiocarbon 59, 695–704.
Curry, R.G., McCartney, M.S., Joyce, T.M., 1998. Oceanic transport of subpolar climate signals to mid-depth subtropical waters. Nature 391, 575–577.
Davies, T.T., Hooper, P.R., 1963. The determination of the calcite-aragonite ratio in mollusc shells by X-ray diffraction. Mineral. Mag. 33, 608–612.
De Clippele, L.H., Huvenne, V.A.I., Molodtsova, T.N., Roberts, J.M., 2019. The diversity and ecological role of non-scleracinian corals (Antipatharia and Alcyonacea) on scleractinian cold-water coral mounds. Front. Mar. Sci. 6, 184.
De la Torriente, A., Serrano, A., Fernández-Salas, L.M., García, M., Aguilar, R., 2018. Identifying epibenthic habitats on the Seco de los Olivos Seamount: Species assemblages and environmental characteristics. Deep Sea Res. Part I 135, 9–22.
DeVries, T., Weber, T., 2017. The export and fate of organic matter in the ocean: new constraints from combining satellite and oceanographic tracer observations. Global Biogeochem. Cycles 31, 535–555.
Du Preez, C., Curtis, J.M., Clarke, M.E., 2016. The structure and distribution of benthic communities on a shallow seamount (Cobb Seamount, Northeast Pacific Ocean). PLoS One 11, 10.
Du Preez, C., Swan, K.D., Curtis, J.M., 2020. Cold-water corals and other vulnerable biological structures on a North Pacific seamount after half a century of fishing. Front. Mar. Sci. 7, 17.
Edwards, R.L., 1988. High Precision Thorium-230 Ages of Corals and the Timing of Sea Level Fluctuations in the Late Quaternary. Ph.D. Thesis, California Institute of Technology.
Eltgroth, S.F., Adkins, J.F., Robinson, L.F., Southon, J., Kashgarian, M., 2006. A deep-sea coral record of North Atlantic radiocarbon through the Younger Dryas: evidence for intermediate water/deepwater reorganization. Paleoceanography 21, PA4207.
FAO, 2009. International Guidelines for the Management of Deep-Sea Fisheries in the High Seas, p. 73. Rome.
Fawcett, S.E., Lomas, M.W., Ward, B.B., Sigman, D.M., 2014. The counterintuitive effect of summer-to-fall mixed layer deepening on eukaryotic new production in the Sargasso Sea. Global Biogeochem. Cycles 28, 86–102.
Feucher, C., Garcia-Quintana, Y., Yashayaev, I., Hu, X., Myers, P.G., 2019. Labrador Sea water formation rate and its impact on the local meridional overturning circulation journal of geophysical research. Oceans 124, 5654–5670.
Freeman, E., Skinner, L.C., Waelbroeck, C., Hodell, D., 2016. Radiocarbon evidence for enhanced respired carbon storage in the Atlantic at the Last Glacial Maximum. Nat. Commun. 7, 11998.
Fricke, H., Meischner, D., 1985. Depth limits of Bermudan scleractinian corals: a submersible survey. Mar. Biol. 88, 175–187.
GEBCO, 2023. The GEBCO_2023 Grid - the 2023 compilation of a continuous terrain model of the global oceans and land. British Oceanographic Data Centre. https://www.gebco.net/data_and_products/gridded_bathymetry_data/. (Accessed 14 March 2024).
Gonçalves Neto, A., Palter, J.B., Bower, A., Furey, H., Xu, X., 2020. Labrador Sea water transport across the charlie-gibbs fracture zone. J. Geophys. Res.: Oceans 125, e2020JC016068.
Government of Bermuda, 2022. The State of Bermuda's Waters: a Snapshot of Bermuda's Exclusive Economic Zone (EEZ) from the Coastline to 200 Nautical Miles (Nm). Government of Bermuda, Ministry of Home Affairs, p. 43. + Appendices A–H.
Grassle, J.P., Sanders, H.L., Hessler, R.R., Rowe, G.T., McLellan, T., 1975. Pattern and zonation: a study of the bathyal megafauna using the research submersible Alvin. Deep-Sea Res. 22, 457–481.
Grigg, R.W., 1997. Benthic communities on Lo'ihi submarine volcano reflect high-disturbance environment. Pac. Sci. 51, 209–220.
Gutjahr, M., Frank, M., Stirling, C.H., Keigwin, L.D., Halliday, A.N., 2008. Tracing the Nd isotope evolution of North Atlantic deep and intermediate waters in the western North Atlantic since the last glacial maximum from Blake Ridge sediments. Earth Planet Sci. Lett. 266, 61–77.
Haedrich, R.L., Rowe, G.T., Polloni, P.T., 1975. Zonation and faunal composition of epibenthic populations on the continental slope south of New England. J. Mar. Res. 33, 191–212.
Hallett, J., 2011. The importance of the Sargasso Sea and the offshore waters of the Bermudian exclusive economic zone to Bermuda and its people. Sargasso Sea Alliance Science Report Series 4, 18.
Heaton, T.J., Kohler, P., Butzin, M., Bard, E., Reimer, R.W., Austin, W.E.N., Ramsey, C.B., Grootes, P.M., Hughen, K.A., Kromer, B., Reimer, P.J., Adkins, J., Burke, A., Cook, M. S., Olsen, J., Skinner, L.C., 2020. Marine20—the marine radiocarbon age calibration curve (0–55,000 cal BP). Radiocarbon 62, 779–820.
Heinrich, H., 1988. Origin and consequences of cyclic ice rafting in the northeast Atlantic Ocean during the past 130,000 years. Quat. Res. 29, 142–152.
Hélie, J.-F., Hillaire-Marcel, C., 2013. Suitability of IAEA-603 as Replacement to NBS19 for Very Small $CaCO_3$-Sample Analysis, p. 11. Report to IAEA- UQAM. https://nucleus.iaea.org/rpst/ReferenceProducts/ReferenceMaterials/Stable_Isotopes/13C18and7Li/IAEA-603/GEOTOP_IAEA-603_Report_2013.pdf.
Hemleben, C., Zahn, R., Meischner, D., 1998. Meteor-Berichte 98-3. Karibik 1996 Cruise No. 35, 18April–3 June 1996.
Hemming, S.R., 2004. Heinrich events: massive late Pleistocene detritus layers of the North Atlantic and their global climate imprint. Rev. Geophys. 42, RG1005.
Hendry, K.R., Robinson, L.F., McManus, J.F., Hays, J.D., 2014. Silicon isotopes indicate enhanced carbon export efficiency in the North Atlantic during deglaciation. Nat. Commun. 5, 3107.
Henry, L.-A., Vad, J., Findlay, H.S., Murillo, J., Milligan, R., Roberts, J.M., 2014. Environmental variability and biodiversity of megabenthos on the Hebrides Terrace Seamount (Northeast Atlantic) nature scientific reports, vol. 4, p. 5589.
Henson, S.A., Sanders, R., Madsen, E., 2012. Global patterns in efficiency of particulate organic carbon export and transfer to the deep ocean. Global Biogeochem. Cycles 26, GB1028.
Hestetun, J.T., Pomponi, S.A., Rapp, H.T., 2016. The cladorhizid fauna (Porifera, Poecilosclerida) of the Caribbean and adjacent waters. Zootaxa 4175, 521–538.
Hillaire-Marcel, C., de Vernal, A., Bilodeau, G., Weaver, A.J., 2001. Absence of deep-water formation in the Labrador Sea during the last interglacial period. Nature 410, 1073–1077.
Hillaire-Marcel, C., de Vernal, A., Bilodeau, G., Wu, G.-P., 1994. Isotope stratigraphy, sedimentation rate and paleoceanographic changes in the Labrador Sea. Can. J. Earth Sci. 31, 63–89.
Hillaire-Marcel, C., Kim, S.T., Landais, A., Ghosh, A., Assonov, S., Lécuyer, C., Blanchard, M., Meijer, H.A.J., Steen-Larsen, H.C., 2021. A stable isotope toolbox for water and inorganic carbon cycle studies. Nat. Rev. Earth Environ. 2, 699–719.
Höfer, J., González, H.E., Laudien, J., Schmidt, G.M., Häussermann, V., Richter, C., 2018. All you can eat: the functional response of the cold-water coral *Desmophyllum dianthus* feeding on krill and copepods. PeerJ 6, e5872.
Howe, J.N.W., Piotrowski, A.M., Noble, T.L., Mulitza, S., Chiessi, C.M., Bayon, G., 2016. North atlantic deep water production during the last glacial maximum. Nat. Commun. 7, 11765.
Iliffe, T.M., 2012. Diving investigations of Bermuda's deep water caves. Nat. Croat. 21, 64–67.
Jaccard, S.L., Galbraith, E.D., 2012. Large climate-driven changes of oceanic oxygen concentrations during the last deglaciation. Nat. Geosci. 5, 151–156.
Jacobsen, S.B., Wasserburg, G.J., 1980. Sm-Nd isotopic evolution of chondrites. Earth Planet Sci. Lett. 50, 139–155.
Kaiser, C.L., Yoerger, D.R., Kinsey, J.C., Kelley, S., Billings, A., Fujii, J., Suman, S., Jakuba, M., Berkowitz, Z., German, C.R., Bowen, A.D., 2016. The Design and 200 Day Per Year Operation of the Autonomous Underwater Vehicle *Sentry*. 2016 IEEE/OES Autonomous Underwater Vehicles (AUV), Tokyo, Japan, pp. 251–260, 2016.
Kenchington, E., Beazley, L., Yashayaev, I., 2017. Hudson 2016-019 international Deep Sea Science expedition cruise report. Can. Data Rep. Fish. Aquat. Sci. 1277, 55.
Kieke, D., Yashayaev, I., 2015. Studies of Labrador Sea Water formation and variability in the subpolar North Atlantic in the light of international partnership and collaboration. Prog. Oceanogr. 132, 220–232.
Lambelet, M., Van De Flierdt, T., Crocket, K., Rehkämper, M., Kreissig, K., Coles, B., Rijkenberg, M.J., Gerringa, L.J., de Baar, H.J., Steinfeldt, R., 2016. Neodymium isotopic composition and concentration in the western North Atlantic Ocean: results from the GEOTRACES GA02 section. Geochem. Cosmochim. Acta 177, 1–29.
Lapointe, A., Watling, L., Gontz, A.M., 2020. Chapter 57 – deep-sea benthic megafaunal communities on the new England and corner rise seamounts, Northwest Atlantic ocean. In: Seafloor Geomorphology as Benthic Habitat, second ed. GeoHab Atlas of Seafloor Geomorphic Features and Benthic Habitats 2020, pp. 917–932.
Lazier, J.R., 1980. Oceanographic conditions at ocean weather ship *Bravo*, 1964–1974. Atmos.-Ocean 18, 227–238.
Le Bras, I.A., Yashayaev, I., Toole, J.M., 2017. Tracking Labrador Sea Water property signals along the deep western boundary current. Journal of Geophysical Research, Oceans 122, 5348–5366.
Legendre, P., Gallagher, E.D., 2001. Ecologically meaningful transformations for ordination of species data. Oecologia 129, 271–280.
Leitner, A.B., Neuheimer, A.B., Drazen, J.C., 2020. Evidence for long-term seamount-induced chlorophyll enhancements. Sci. Rep. 10, 1–10.
Levin, L.A., Rouse, G.W., 2019. Giant protists (xenophyophores) function as fish nurseries. Ecology 101, e02933.
Levin, L.A., Thomas, C.L., 1988. The ecology of xenophyophores (Protista) on eastern Pacific seamounts. Deep-Sea Res. 35, 2003–2027.
Lomas, M.W., Bates, N.R., Johnson, R.J., Knap, A.H., Steinberg, D.K., Carlson, C.A., 2013. Two decades and counting: 24-years of sustained open ocean biogeochemical measurements in the Sargasso Sea. Deep-Sea Res. Part II 93, 16–32.
Ludwig, K.R., 2003. User's manual for Isoplot 3.00: a geochronological toolkit for microsoft Excel. Berkeley Geochronology Center Special publication 4.
Lynch-Stieglitz, J., Schmidt, M.W., Henry, G.L., Curry, W.B., Skinner, L.C., Mulitza, S., Zhang, R., Chang, P., 2014. Muted change in Atlantic overturning circulation over some glacial-aged Heinrich events. Nat. Geosci. 7, 144–150.
Maccali, J., Hillaire-Marcel, C., Ghaleb, B., Ménabréaz, L., Blénet, A., Edinger, E., Hélie, J.-F., Preda, M., 2020. Late Quaternary sporadic development of *Desmophyllum dianthus* deep-coral populations in the southern Labrador Sea with specific attention to their ^{14}C- and ^{230}Th-dating. Mar. Chem. 224, 103807.
Marali, S., Wisshak, M., Correa, M.L., Freiwald, A., 2013. Skeletal microstructure and stable isotope signature of three bathyal solitary cold-water corals from the Azores. Palaeogeography, Palaeoclimatology. Palaeoecology 373, 25–38.
Martínez-Dios, A., Pelejero, C., López-Sanz, À., Sherrell, R.M., Ko, S., Häussermann, V., Försterra, G., Calvo, E., 2020. Effects of low pH and feeding on calcification rates of the cold-water coral *Desmophyllum dianthus*. PeerJ 8, e8236.
Meredyk, S.P., 2017. Physical Characterization and Benthic Megafauna Distribution and Species Composition on Orphan Knoll and Orphan Seamount, NW Atlantic. MSc thesis, Memorial University, Newfoundland.

Morato, T., et al., 2020. Climate-induced changes in the suitable habitat of cold-water corals and commercially important deep-sea fishes in the North Atlantic. Global Change Biol. 26, 2181–2202.
Morgan, N.B., Goode, S., Roark, E.B., Baco, A.R., 2019. Fine scale assemblage structure of benthic invertebrate megafauna on the North Pacific seamount Mokumanamana. Front. Mar. Sci. 6, 715.
Mullineau, L.S., Mills, S.W., 1997. A test of the larval retention hypothesis in seamount-generated flows. Deep Sea Res. Oceanogr. Res. Pap. 44, 745–770.
O'Nions, R.K., Carter, S.R., Cohen, R.S., Evensen, N.M., Hamilton, P.J., 1978. Pb, Nd and Sr isotopes in oceanic ferromanganese deposits and ocean floor basalts. Nature 273, 435–438.
Parson, L., Edwards, R., 2011. The geology of the Sargasso Sea Alliance study area, potential non-living marine resources and an overview of the current territorial claims and coastal states interests. Sargasso Sea Alliance Science Report Series 8, 17.
Phillips, H.E., Joyce, T.M., 2007. Bermuda's tale of two time series: Hydrostation S and BATS. J. Phys. Oceanogr. 37, 554–571.
Pin, C., Zalduegui, J.S., 1997. Sequential separation of light rare-earth elements, thorium and uranium by miniaturized extraction chromatography: application to isotopic analyses of silicate rocks. Anal. Chim. Acta 339, 79–89.
Pitcher, T.J., Clark, M.R., Morato, T., Watson, R., 2010. Seamount fisheries: do they have a future? Oceanography 23, 134–144.
Pratt, R.M., 1962. The ocean bottom. Science 138, 492–495.
Pratt, R.M., 1967. Photography of seamounts. In: Hersey, J.B. (Ed.), Deep-sea Photography. WHOI Technical Report 71–15. Johns Hopkins Oceanographic Studies No. 3.
Puerta, P., Johnson, C., Carreiro-Silva, M., Henry, L.-A., Kenchington, E., Morato, T., Kazanidis, G., Rueda, J.L., Urra, J., Ross, S., González-Irusta, J.-M., Arnaud-Haond, S., Orejas, C., 2020. Influence of water masses on the biodiversity and biogeography of deep-sea benthic ecosystems in the North Atlantic. Front. Mar. Sci. 7, 239.
Ramiro-Sánchez, B., González-Irusta, J.M., Henry, L.-A., Cleland, J., Yeo, I., Xavier, J.R., Carreiro-Silva, M., Sampaio, Í., Spearman, J., Victorero, L., Messing, C.G., Kazanidis, G., Roberts, J.M., Murton, B., 2019. Characterization and mapping of a deep-sea sponge ground on the Tropic Seamount (Northeast tropical Atlantic): implications for spatial management in the High Seas. Front. Mar. Sci. 6, 278.
Reimer, P.J., Bard, E., Bayliss, A., Beck, J.W., Blackwell, P.G., Ramsey, C.B., Buck, C.E., Cheng, H., Edwards, R.L., Friedrich, M., Grootes, P.M., 2013. IntCal13 and Marine13 radiocarbon age calibration curves 0–50,000 years cal BP. Radiocarbon 55, 1869–1887.
Ressurreição, A., Giacomello, E., 2013. Quantifying the direct use value of Condor seamount. Deep Sea Res. Part II 98, 209–217.
Rhein, M., Steinfeldt, R., Kieke, D., Stendardo, I., Yashayaev, I., 2017. Ventilation variability of Labrador Sea Water and its impact on oxygen333 and anthropogenic carbon: a review. Philosophical Transactions of the Royal Society A 375, 20160321.
Roberts, J.M., Henry, L.-A., Long, D., Hartley, J.P., 2008. Cold-water coral reef frameworks, megafaunal communities and evidence for coral carbonate mounds on the Hatton Bank, north east Atlantic. Facies 54, 297–316.
Robinson, L.F., Adkins, J.F., Scheirer, D.S., Fernandez, D.P., Gagnon, A., Waller, R.G., 2007. Deep-sea scleractinian coral age and depth distributions in the Northwest Atlantic for the last 225,000 years. Bull. Mar. Sci. 81, 371–391.
Saenger, C., Gabitov, R.I., Farmer, J., Watkins, J.M., Stone, R., 2017. Linear correlations in bamboo coral $\delta^{13}C$ and $\delta^{18}O$ sampled by SIMS and micromill: evaluating paleoceanographic potential and biomineralization mechanisms using $\delta^{11}B$ and Δ_{47} composition. Chem. Geol. 454, 1–14.
Shepherd, J.G., Brewer, P.G., Oschlies, A., Watson, A.J., 2017. Ocean ventilation and deoxygenation in a warming world: introduction and overview. Philosophical Transactions of the Royal Society A 375, 20170240.
Sinclair, D.J., Williams, B., Allard, G., Ghaleb, B., Fallon, S., Ross, S.W., Risk, M., 2011. Reproducibility of trace element profiles in a specimen of the deep-water bamboo coral *Keratoisis* sp. Geochem. Cosmochim. Acta 75, 5101–5121.
Smith, C.R., Hamilton, S.C., 1983. Epibenthic megafauna of a bathyal basin off southern California: patterns of abundance, biomass, and dispersion. Deep-Sea Res. 30, 907–928.
Smith, J.E., Risk, M.J., Schwarcz, H.P., McConnaughey, T.A., 1997. Rapid climate change in the North Atlantic during the Younger Dryas recorded by deep-sea corals. Nature 386, 818–820.
Smith, J.N., Smethie Jr., W.M., Yashayev, I., Curry, R., Azetsu-Scott, K., 2016. Time series measurements of transient tracers and tracer-derived transport in the deep western boundary current between the labrador Sea and the subtropical Atlantic Ocean at line W. Journal of Geophysical Research Oceans 121, 8115–8138.
Spalding, M., Fos, H., Allen, G., Davidson, N., Ferdaña, Z., Finlayson, M., Halpern, B.S., Jorge, M.A., Lomgana, A., Lourie, S.A., Martin, K.D., McManus, E., Molnar, J., Recchia, C.A., Robertson, J., 2007. Marine ecoregions of the world: a bioregionalization of coastal and shelf areas. Bioscience 57, 573–583.
Stefanoudis, P.V., Gress, E., Pitt, J.M., Smith, S.R., Kincaid, T., Rivers, M., Andradi-Brown, D.A., Rowlands, G., Woodall, L.C., Rogers, A.D., 2019a. Depth-dependent structuring of reef fish assemblages from the shallows to the rariphotic zone. Front. Mar. Sci. 6, 307.
Stefanoudis, P.V., Rivers, M., Smith, S.R., Schneider, C.W., Wagner, D., Ford, H., Rogers, A.D., Woodall, L.C., 2019b. Low connectivity between shallow, mesophotic and rariphotic zone benthos. R. Soc. Open Sci. 6, 190958.
Steinberg, D.K., Carlson, C.A., Bates, N.R., Johnson, R.J., Michaels, A.F., Knap, A.H., 2001. Overview of the US JGOFS Bermuda Atlantic Time Series (BATS): a decade scale look at ocean biology and biogeochemistry. Deep-Sea Research II 48, 1405–1447.
Stuiver, M., Polach, H.A., 1977. Discussion: reporting of ^{14}C data. Radiocarbon 19, 355–363.
Stuiver, M., Reimer, P., 1993. Extended ^{14}C data base and revised CALIB 3.0 ^{14}C age calibration program. Radiocarbon 35, 215–230.
Sweetman, A.K., Thurber, A.R., Smith, C.R., Levin, L.A., Mora, C., Wei, C.-L., Gooday, A. J., Jones, D.O.B., Rex, M., Yasuhara, M., Ingels, J., Ruhl, H.A., Frieder, C.A., Danovaro, R., Würzberg, L., Baco, A., Grupe, B.M., Pasulka, A., Meyer, K.S., Dunlop, K.M., Henry, L.-A., Roberts, J.M., 2017. Major impacts of climate change on deep-sea benthic ecosystems. Elementa: Science of the Anthropocene 5, 4.
Tanaka, T., Togashi, S., Kamioka, H., Amakawa, H., Kagami, H., Hamamoto, T., Yuhara, M., Orihashi, Y., Yoneda, S., Shimizu, H., Kunimaru, T., 2000. JNdi-1: a neodymium isotopic reference in consistency with La Jolla neodymium. Chem. Geol. 168, 279–281.
Thiagarajan, N., Gerlach, D., Roberts, M.L., Burke, A., McNichol, A., Jenkins, W.J., Subhas, A.V., Thresher, R.E., Adkins, J.F., 2013. Movement of deep-sea coral populations on climatic timescales. Paleoceanography 28, 227–236.
Thoma, J.N., Pante, E., Brugler, M.R., France, S.C., 2009. Deep-sea octocorals and antipatharians show no evidence of seamount-scale endemism in the NW Atlantic. Mar. Ecol. Prog. Ser. 397, 25–35.
Tittensor, D.P., Baco, A.R., Brewin, P.E., Clark, M.R., Consalvey, M., Hall-Spencer, J., Rowden, A.A., Schlacher, T., Stocks, K.I., Rogers, A.D., 2009. Predicting global habitat suitability for stony corals on seamounts. J. Biogeogr. 36, 1111–1128.
van de Flierdt, T., Robinson, L.F., Adkins, J.F., 2010. Deep-sea coral aragonite as a recorder for the neodymium isotopic composition of seawater. Geochem. Cosmochim. Acta 74, 6014–6032.
Vianello, P., Herbette, S., Ternon, J.F., Demarcq, H., Roberts, M.J., 2020. Observation of a mesoscale eddy dipole on the northern Madagascar Ridge: consequences for the circulation and hydrography in the vicinity of a seamount. Deep Sea Res. Part II 176, 104815.
Victorero, L., Robert, K., Robinson, L.F., Taylor, M.L., Huvenne, V.A., 2018. Species replacement dominates megabenthos beta diversity in a remote seamount setting. Nature Scientific Reports 8, 4152.
Vogt, P.R., Jung, W.Y., 2007. Origin of the Bermuda volcanoes and the Bermuda Rise: history, observations, models, and puzzles. In: Foulger, G.R., Jurdy, D.M. (Eds.), Plates, Plumes and Planetary Processes. Geological Society America Special Paper no. 430, Geological Society of America, Boulder, pp. 553–591.
Wacker, L., Hajdas, I., Friedrich, M., 2010. MICADAS: routine and high precision radiocarbon dating. Radiocarbon 52, 252–262.
Wang, X.T., Prokopenko, M.G., Sigman, D.M., Adkins, J.F., Robinson, L.F., Ren, H., Oleynik, S., Williams, B., Haug, G.H., 2014. Isotopic composition of carbonate-bound organic nitrogen in deep-sea scleractinian corals: a new window into past biogeochemical change. Earth Planet Sci. Lett. 400, 243–250.
Watling, L., Auster, P.J., 2017. Seamounts on the high seas should be managed as vulnerable marine ecosystems. Front. Mar. Sci. 4, 14.
Wilson, M.F.J., O'Connell, B., Brown, C., Guinan, J.C., Grehan, A.J., 2007. Multiscale terrain analysis of multibeam bathymetry data for habitat mapping on the continental slope. Mar. Geodesy 30, 3–35.
Wentworth, C.K., 1922. A scale of grade and class terms for clastic sediments. J. Geol. 30, 377–392.
Wong, A.P., Wijffels, S.E., Riser, S.C., Pouliquen, S., Hosoda, S., Roemmich, D., Gilson, J., Johnson, G.C., Martini, K., Murphy, D.J., Scanderbeg, M., 2020. Argo data 1999–2019: two million temperature-salinity profiles and subsurface velocity observations from a global array of profiling floats. Front. Mar. Sci. 7, 700.
Yashayaev, I., 2024. Intensification and shutdown of deep convection in the Labrador Sea were caused by changes in atmospheric and freshwater dynamics. Nature Communications Earth and Environment. https://doi.org/10.1038/s43247-024-01296-9.
Yashayaev, I., Bersch, M., van Aken, H.M., 2007. Spreading of the Labrador Sea Water to the irminger and Iceland basins. Geophys. Res. Lett. 34, L10602.
Yashayaev, I., Dickson, B., 2008. Transformation and fate of overflows in the northern North Atlantic. In: Dickson, R.R., Meincke, J., Rhines, P. (Eds.), Arctic–Subarctic Ocean Fluxes. Springer, Dordrecht, pp. 505–526.
Yashayaev, I., Loder, J.W., 2016. Recurrent replenishment of Labrador Sea Water and associated decadal-scale variability. Journal of Geophysical Research Oceans 121, 8095–8114.
Yashayaev, I., Loder, J.W., 2017. Further intensification of deep convection in the Labrador Sea in 2016. Geophys. Res. Lett. 44, 1429–1438.
Yashayaev, I., Peterson, I., Wang, Z., 2022. Meteorological, Sea Ice, and Oceanographic Conditions in the Labrador Sea during 2020. Canadian Science Advisory Secretariat (CSAS) Research Document 2022/039. Maritimes Region, Fisheries and Oceans Canada, p. 62.
Yashayaev, I.M., Zveryaev, I.I., 2001. Climate of the seasonal cycle in the North pacific and the North atlantic oceans. Int. J. Climatol.: A Journal of the Royal Meteorological Society 21, 401–417.
Yesson, C., Taylor, M.L., Tittensor, D.P., Davies, A.J., Guinotte, J., Baco, A., Black, J., Hall-Spencer, J., Rogers, A.D., 2012. Global habitat suitability of cold-water octocorals. J. Biogeogr. 39, 1278–1292.
Ziveri, P., Stoll, H., Probert, I., Klaas, C., Geisen, M., Ganssen, G., Young, J., 2003. Stable isotope 'vital effects' in coccolith calcite. Earth Planet Sci. Lett. 210, 137–149.